

# Fast Nonseparable Gaussian Stochastic Process with Application to Methylation Level Interpolation

Mengyang Gu\* and Yanxun Xu\*\*

\* Department of Statistics and Applied Probability, University of California, Santa Barbara, CA

\*\* Department of Applied Mathematics and Statistics, Johns Hopkins University, Baltimore, MD

## Abstract

Gaussian stochastic process (GaSP) has been widely used as a prior over functions due to its flexibility and tractability in modeling. However, the computational cost in evaluating the likelihood is  $O(n^3)$ , where  $n$  is the number of observed points in the process, as it requires to invert the covariance matrix. This bottleneck prevents GaSP being widely used in large-scale data. We propose a general class of nonseparable GaSP models for multiple functional observations with a fast and exact algorithm, in which the computation is linear ( $O(n)$ ) and exact, requiring no approximation to compute the likelihood. We show that the commonly used linear regression and separable models are special cases of the proposed nonseparable GaSP model. Through the study of an epigenetic application, the proposed nonseparable GaSP model can accurately predict the genome-wide DNA methylation levels and compares favorably to alternative methods, such as linear regression, random forest and localized Kriging method. The algorithm for fast computation is implemented in the `FastGaSP` R package on CRAN. KEY WORDS: Exact computation, Fast algorithm, Methylation levels imputation, Multiple functional data, Stochastic differential equations

# 1 Introduction

The increasing demands to analyze high dimensional data with complex structures have facilitated the development of novel statistical models for functional data, in which the outcomes can be interpreted as samples of random functions. Time series, longitudinal, and spatial data are some typical examples of functional data. One common feature among functional data is that, often, the linear regression does not appropriately explain the correlations between the outcomes that are close in the inputs of the function. The correlation is often expressed through a mapping from the functional inputs to the associated outcomes, usually modeled as a stochastic process, and the correlations between nearby inputs are captured through a covariance matrix. One natural choice of such stochastic process is the Gaussian stochastic process (GaSP), which has been widely used in many applications (Sacks et al., 1989; Bayarri et al., 2009; Gelfand et al., 2010).

GaSP models have also been popular in analyzing functional data with multiple functional outcomes, in which independent GaSP models are generally built separately for each outcome for simplicity. A more sophisticated approach is to define a separable GaSP model, where the correlations between functions and between inputs are modeled separately using a matrix normal distribution (Conti and O’Hagan, 2010). Other approaches include the use of a linear model of coregionalization, where the factor processes modeled as independent GaSPs to explain the variation over the input space. This construction results in *nonseparable* covariance structures, meaning that the covariance matrix cannot be decomposed as a Kronecker product of two small covariance matrices.

For large-scale data, a GaSP model is often computationally expensive: the evaluation of the likelihood requires  $O(n^3)$  computational operations to compute the inverse of the covariance matrix, where  $n$  is the number of observed data points. To ease the computation, many approximation methods have been proposed, including low rank approximation

(Banerjee et al., 2008), covariance tapering (Kaufman et al., 2008), use of Gaussian Markov random field representations (Lindgren et al., 2011), and likelihood approximation (Eidsvik et al., 2013). Those approximation methods are sometimes preferred for computationally intensive problems, however, the exact computation is more desired if we can overcome the  $O(n^3)$  computational operations.

Our motivating study is to impute millions of DNA methylation levels at CpG sites across the human genome. DNA methylation is an epigenetic modification of DNA, playing important roles in DNA replication, gene transcription, aging, and cancer evolution (Das and Singal, 2004; Scarano et al., 2005). Methylation levels are quantified at every genomic CpG site, a region of DNA where a cytosine (C) nucleotide is followed by a guanine (G) nucleotide in the linear sequence of bases along its 5' to 3' direction. Single-site DNA methylation level can be quantified by whole-genome bisulfite sequencing (WGBS), in which approximately 26 million CpG sites in the human genome are evaluated for whether they are methylated or not. However, WGBS is expensive and hard to examine in certain genomic regions. This motivates alternative methylation assay technologies, such as Illumina HumanMethylation450 BeadChip (henceforth, Methylation450K) that measures DNA methylation levels at approximately 482,000 CpG sites (less than 2% of the total number of CpG sites). The goal is to impute DNA methylation levels at the CpG sites that are observed in the WGBS samples but unobserved in the Methylation450K data by exploiting the correlations among the full set of CpG sites in the WGBS samples.

We first explore the empirical correlation of methylation levels studied in the WGBS data (Ziller et al., 2013). For each integer distance smaller than 5000 bases, we plot the empirical correlation of every possible pair with this distance in the left panel of Figure 1. The blue dots are the average correlation of the methylation levels between two CpG sites at a given CpG distance smaller than 5000 bases. The methylation levels at nearby CpG sites are correlated to each other on average and the correlation gradually decays as the distance

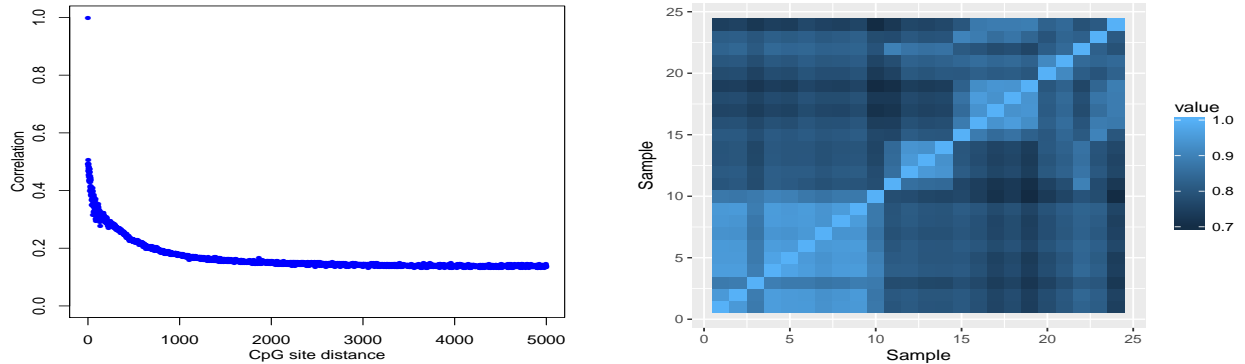


Figure 1: Empirical correlation of methylation levels across sites (left panel) and across samples (right panel), based on 24 samples and one million methylation levels in chromosome 1 of each sample.

between the two CpG sites increases. Such phenomenon is called co-methylation and has been observed in previous studies (Zhang et al., 2015). Furthermore, we plot the correlation of the methylation levels across samples in the right panel of Figure 1 (Wickham, 2016, 2007), which shows the methylation levels are highly correlated for biological reasons. Since methylation plays important roles in suppressing gene expression levels, they are tightly regulated in cells and variability of such regulations is associated with disease risk (Das and Singal, 2004). Understanding the correlation patterns in methylations levels is thus meaningful for reducing the risk of diseases. These empirical findings motivate us to develop a statistical model to exploit the correlations of methylation levels across the unequally-spaced genome sites and across different samples for the goal of imputation.

In this paper, we develop a computationally efficient model to impute the methylation levels. Our contribution lies in both application and methodology. First, we propose to use a nonseparable GaSP model to integrate different correlation structures among the methylation levels across genome sites and across samples into a coherent model, while the previous regression method in Zhang et al. (2015) ignores the correlations across samples. To achieve this goal, we propose a computationally approach for the nonseparable model in Higdon et al. (2008). We first show that the marginal likelihood of this model can be written as a product

of the multivariate normal distributions of the transformed output, and then we apply the forward filtering and backward smoothing algorithm for the GaSP with a Matérn kernel function (Hartikainen and Sarkka, 2010). In our algorithm, the computational operations and storage are linear to the number of observations without an approximation to the likelihood function. We implement this algorithm in an R package on CRAN (Gu, 2019a) based on the R software (R Core Team, 2019). Lastly, we show that the proposed nonseparable GaSP model is a general statistical framework that unifies the linear regression and separable GaSP models.

The rest of the paper is organized as follows. In Section 2, we study a class of nonseparable GaSP models. The closed form marginal likelihood and predictive distribution are derived for the imputation problem. In Section 3, the computational strategy for this class of nonseparable GaSP models is introduced, for which the computation scales linearly in the number of inputs of the function without approximation. In Section 4, we unify some other frequently used approaches, such as the linear regression and separable GaSP models, under the framework of the nonseparable GaSP models. Numerical examples and comparisons to alternative methods are provided in Section 5. We conclude the paper with discussion and future extensions in Section 6.

## 2 Modeling multiple functional data

Let  $y_i(s_j)$  be the methylation level of the  $i^{\text{th}}$  sample at the  $j^{\text{th}}$  CpG site, recording the proportion of probes for a single CpG site that is methylated, for  $i = 1, \dots, K$ ,  $j = 1, \dots, N$ . Define two groups of sites,  $\mathbf{s}^{\mathcal{D}} = \{s_1^{\mathcal{D}}, \dots, s_n^{\mathcal{D}}\}$  and  $\mathbf{s}^* = \{s_1^*, \dots, s_{n^*}^*\}$ , where the methylation levels of  $\mathbf{s}^{\mathcal{D}}$  are observed for all  $K$  samples and the methylation levels of  $\mathbf{s}^* = \{s_1^*, \dots, s_{n^*}^*\}$  are only available for the first  $k$  samples but not available for the last  $k^*$  samples. The total number of samples is  $K = k + k^*$  and the total number of CpG sites is  $N = n + n^*$ .

For the first  $k$  samples, methylation levels are measured at all CpG sites, meaning that we observe  $\mathbf{y}(\mathbf{s}^{\mathcal{D}})_{[k \times n]}$  and  $\mathbf{y}(\mathbf{s}^*)_{[k \times n^*]}$ . However, for the remaining  $k^*$  samples, the methylation levels are only observed at a small subset of CpG sites, denoted as  $\mathbf{y}^*(\mathbf{s}^{\mathcal{D}})_{[k^* \times n]}$ . The methylation levels at the remaining CpG sites ( $\mathbf{y}^*(\mathbf{s}^*)_{[k^* \times n^*]}$ ) of these samples are unknown. Our goal, then, is to interpolate the unobserved methylation levels of these  $k^*$  samples using their observed methylation values at  $n$  CpG sites and the full methylation values from the other  $k$  samples. In other words, we seek the predictive distribution of  $\mathbf{y}^*(\mathbf{s}^*)$  conditional on  $\mathbf{y}(\mathbf{s}^{\mathcal{D}})$ ,  $\mathbf{y}(\mathbf{s}^*)$  and  $\mathbf{y}^*(\mathbf{s}^{\mathcal{D}})$ .

The imputation of methylation levels across the whole genome is computationally challenging due to the large number of CpG sites. In the full WGBS data set, there are about  $2.8 \times 10^7$  CpG sites; even in the smaller Methylation450K data, there are roughly  $4.5 \times 10^5$  CpG sites, creating computational challenges. In contrast, the number of samples we are working with is relatively small: 24 samples in the WGBS data and 100 samples in the Methylation450K data. The key advantage of our method is that the computation required for imputation scales linearly in terms of the number of CpG sites.

Here we make several extensions of a class of GaSP models with the nonseparable structure, which has been used for modeling multivariate spatially correlated data and functional outputs (Goulard and Voltz, 1992; Higdon et al., 2008). First of all, we construct a flexible way to incorporate the correlations across samples and across sites for prediction, with closed form expression of the marginal likelihood and predictive distribution. These expressions enable us to establish the connection between this nonseparable model and other models, such as the linear regression and separable models, discussed in Section 4. Furthermore, we introduce a computationally feasible approach to large-scale problems with inputs (CpG sites) up to a million without approximating the likelihood function. This computational feasible approach depends on the explicit form of the likelihood in Lemma 1, which can be computed linearly to the number of samples. We further give an exact and fast computation in Section

3 such that the overall computation of the likelihood is exact and at the order of  $O(nK)$  operations, rather than  $O((nK)^3)$  operations. The proof of this section is given in Appendix. Without loss of generality, we assume the data are centered at zero. An extension to combine site-specified features is given in the supplementary materials.

## 2.1 Nonseparable GaSP model

We start with the linear model of coregionalization (LMC) of the outputs  $\mathbf{Y}(s)$ , a  $K \times 1$  vector for every site  $s \in \mathcal{S}$  (Goulard and Voltz (1992); Gelfand et al. (2004); Higdon et al. (2008); Chang et al. (2014)):

$$\mathbf{Y}(s) = \mathbf{A}\tilde{\mathbf{v}}(s) + \boldsymbol{\epsilon}_0, \quad (1)$$

where  $\boldsymbol{\epsilon}_0 \sim \text{MN}(\mathbf{0}, \sigma_0^2 \mathbf{I}_K)$ ,  $\mathbf{A} = (\mathbf{a}_1; \dots; \mathbf{a}_K)$  is a  $K \times K$  matrix with  $\mathbf{a}_i$  being the  $i^{\text{th}}$  factor loading vector ( $K \times 1$  vector) specified later and  $\tilde{\mathbf{v}}(s) = (\tilde{v}_1(s), \dots, \tilde{v}_K(s))^T$  is a vector of random factors at site  $s$ . Note that one may define  $\mathbf{A}$  to be a  $K \times d$  matrix with  $d \leq K$  for other applications, but since  $K$  is small in our application, we do not pursue the dimension reduction toward this direction.

As shown in Figure 1, the correlation of the methylation levels at nearby CpG sites decays as the genomic distance increases. This motivates us to model each random factor processes  $\tilde{v}_i(\cdot)$  independently as a zero mean GaSP with noises for  $s \in \mathcal{S}$ :

$$\begin{aligned} \tilde{v}_i(s) &= v_i(s) + \epsilon_i, \\ v_i(\cdot) &\sim \text{GaSP}(0, \tau_i^2 c_i(\cdot, \cdot)), \end{aligned} \quad (2)$$

where  $\epsilon_i \sim \text{N}(0, \sigma_i^2)$  is an independent noise and  $\tau_i^2 c_i(s_a, s_b)$  is the covariance between any site  $s_a, s_b \in \mathcal{S}$ , with unknown variances  $\sigma_i^2$  and  $\tau_i^2$ , respectively. Denote the nugget variance ratio parameter  $\eta_i = \sigma_i^2 / \tau_i^2$ . Form (2) implies the marginal distribution of  $\tilde{\mathbf{v}}_i(\mathbf{s}^{\mathcal{S}}) =$

$(\tilde{v}_i(s_1^{\mathcal{S}}), \dots, \tilde{v}_i(s_n^{\mathcal{S}}))^T$  follows a multivariate normal distribution below:

$$\tilde{\mathbf{v}}_i(\mathbf{s}^{\mathcal{S}}) \mid \tau_i^2, \eta_i \sim \text{MN}(\mathbf{0}, \tau_i^2(\mathbf{R}_i + \eta_i \mathbf{I}_n)),$$

where the  $(l, m)$  entry of the correlation matrix  $\mathbf{R}_i$  is  $c_i(s_l^{\mathcal{S}}, s_m^{\mathcal{S}})$  for  $i = 1, \dots, K$ , and  $\mathbf{I}_n$  is an  $n \times n$  identity matrix. The Matérn kernel is often used for modeling the correlation:

$$c_i(d) = \frac{1}{2^{\nu_i-1} \Gamma(\nu_i)} \left( \frac{d}{\gamma_i} \right)^{\nu_i} \mathcal{K}_{\nu_i} \left( \frac{d}{\gamma_i} \right), \quad (3)$$

where  $\Gamma(\cdot)$  is the gamma function,  $\mathcal{K}_{\nu_i}(\cdot)$  is the modified Bessel function of the second kind with a smoothness parameter  $\nu_i$ ,  $\gamma_i$  is a range parameter, and  $d = |s_a - s_b|$  for any  $s_a, s_b \in \mathcal{S}$ . When  $\nu_i = (2m_i + 1)/2$  with  $m_i \in \mathbb{N}$ , the GaSP with a Matérn kernel is  $m_i^{\text{th}}$  sample path differentiable and the Matérn kernel has a closed form expression in these scenarios. For instance, the exponential kernel is equivalent to the Matérn kernel with  $\nu_i = 1/2$  and the Gaussian kernel is the Matérn kernel with  $\nu_i \rightarrow +\infty$ . The flexibility of the Matérn kernel makes it widely applicable for modeling spatially correlated data (Gelfand et al., 2010).

Denote  $\mathbf{Y}(\mathbf{s}^{\mathcal{S}}) = (\mathbf{y}(\mathbf{s}^{\mathcal{S}})^T; \mathbf{y}^*(\mathbf{s}^{\mathcal{S}})^T)^T$ . Following Higdon et al. (2008), we apply the singular value decomposition (SVD) to  $\mathbf{Y}(\mathbf{s}^{\mathcal{S}}) = \mathbf{U}\mathbf{D}\mathbf{V}$  and estimate  $\mathbf{A}$  as  $\mathbf{A} = \mathbf{U}\mathbf{D}/\sqrt{n}$ , for the following reasons. First of all, the computational order of estimating  $\mathbf{A}$  is linear to  $n$ , which is essential when  $n$  is at the size of  $10^6$ . Secondly, we have  $\mathbf{a}_i^T \mathbf{a}_j = 0$  if  $i \neq j$ , and hence  $\mathbf{A}^T \mathbf{A}$  is a diagonal matrix, which substantially simplifies the computation of the likelihood. Moreover,  $\mathbf{A}\mathbf{A}^T = \mathbf{Y}(\mathbf{s}^{\mathcal{S}})\mathbf{Y}(\mathbf{s}^{\mathcal{S}})^T/n$ , unifying the linear regression model under the framework of the nonseparable model shown later in Remark 1 of Section 4.

Denote the  $K \times n$  factor matrix  $\tilde{\mathbf{v}}(\mathbf{s}^{\mathcal{S}})$  with the  $(i, j)$  term being  $\tilde{v}_i(s_j^{\mathcal{S}})$  for  $1 \leq i \leq K$  and  $1 \leq j \leq n$ . Note the  $\tilde{\mathbf{v}}(\mathbf{s}^{\mathcal{S}})$  can be marginalized explicitly. We first vectorize the outputs  $\mathbf{Y}_v(\mathbf{s}^{\mathcal{S}}) := \text{vec}(\mathbf{Y}(\mathbf{s}^{\mathcal{S}}))$  and factor matrix  $\tilde{\mathbf{v}}_v(\mathbf{s}^{\mathcal{S}}) := \text{vec}(\tilde{\mathbf{v}}(\mathbf{s}^{\mathcal{S}})^T)$ , both of which are  $Kn$ -dimensional vectors. Define a  $Kn \times Kn$  matrix  $\mathbf{A}_v := [\mathbf{I}_n \otimes \mathbf{a}_1; \dots; \mathbf{I}_n \otimes \mathbf{a}_K]$ . By simple



algebra, model (1) can be written as

$$\mathbf{Y}_v(\mathbf{s}^{\mathcal{D}}) = \mathbf{A}_v \tilde{\mathbf{v}}_v(\mathbf{s}^{\mathcal{D}}) + \boldsymbol{\epsilon}_{0v}, \quad (4)$$

where  $\boldsymbol{\epsilon}_{0v} \sim \text{MN}(\mathbf{0}, \sigma_0^2 \mathbf{I}_{nK})$  and  $(\tilde{\mathbf{v}}_v(\mathbf{s}^{\mathcal{D}}) \mid \tau_1^2, \dots, \tau_K^2, \tilde{\mathbf{R}}_1, \dots, \tilde{\mathbf{R}}_K) \sim \text{MN}(\mathbf{0}, \boldsymbol{\Sigma}_v)$ , with the  $(l, m)$  entry of the  $\tilde{\mathbf{R}}_i$  being  $\tilde{c}_i(s_l^{\mathcal{D}}, s_m^{\mathcal{D}}) = c_i(s_l^{\mathcal{D}}, s_m^{\mathcal{D}}) + \eta_i 1_{l=m}$ . Here  $\boldsymbol{\Sigma}_v = \text{blkdiag}(\tau_1^2 \tilde{\mathbf{R}}_1; \dots; \tau_K^2 \tilde{\mathbf{R}}_K)$ , where  $\text{blkdiag}(\cdot)$  means the block diagonal matrix between sites. As shown in Higdon et al. (2008), directly marginalizing out  $\tilde{\mathbf{v}}_v(\mathbf{s}^{\mathcal{D}})$  leads to:

$$\mathbf{Y}_v(\mathbf{s}^{\mathcal{D}}) \mid \sigma_0^2, \tau_1^2, \dots, \tau_K^2, \tilde{\mathbf{R}}_1, \dots, \tilde{\mathbf{R}}_K \sim \text{MN}(\mathbf{0}, \mathbf{A}_v \boldsymbol{\Sigma}_v \mathbf{A}_v^T + \sigma_0^2 \mathbf{I}_{Kn}). \quad (5)$$

The straightforward computation of the likelihood (5), however, requires to invert a  $Kn \times Kn$  covariance matrix  $\mathbf{A}_v \boldsymbol{\Sigma}_v \mathbf{A}_v^T + \sigma_0^2 \mathbf{I}_{Kn}$ , which takes  $O((Kn)^3)$  operations in general. The following lemma states the likelihood in (5) can be computed with  $O(Kn^3)$  operations.

**Lemma 1.** *Assume  $\mathbf{A} = \mathbf{U}\mathbf{D}/\sqrt{n}$ , where  $\mathbf{U}$  and  $\mathbf{D}$  are from the SVD of  $\mathbf{Y}(\mathbf{s}^{\mathcal{D}}) = \mathbf{U}\mathbf{D}\mathbf{V}$ . After integrating out  $\mathbf{v}(\mathbf{s}^{\mathcal{D}})$ , the marginal likelihood of  $\mathbf{Y}(\mathbf{s}^{\mathcal{D}})$  in model (1) follows a product of  $K$  independent multivariate normal distributions,*

$$p(\mathbf{Y}(\mathbf{s}^{\mathcal{D}}) \mid \sigma_0^2, \tau_1^2, \dots, \tau_K^2, \tilde{\mathbf{R}}_1, \dots, \tilde{\mathbf{R}}_K) = |\mathbf{A}_v^T \mathbf{A}_v|^{-\frac{1}{2}} \prod_{i=1}^K p_{MN}(\hat{\mathbf{v}}_i(\mathbf{s}^{\mathcal{D}}); \mathbf{0}, \tau_i^2 \tilde{\mathbf{R}}_i + \sigma_0^2 (\mathbf{a}_i^T \mathbf{a}_i)^{-1} \mathbf{I}_n),$$

where  $p_{MN}(\cdot; \boldsymbol{\mu}, \boldsymbol{\Sigma})$  denotes the multivariate normal density with mean  $\boldsymbol{\mu}$  and covariance  $\boldsymbol{\Sigma}$ ,  $\hat{\mathbf{v}}_i(\mathbf{s}^{\mathcal{D}})$  is the transpose of the  $i^{\text{th}}$  row of

$$\hat{\mathbf{v}}(\mathbf{s}^{\mathcal{D}}) = (\mathbf{A}^T \mathbf{A})^{-1} \mathbf{A}^T \mathbf{Y}(\mathbf{s}^{\mathcal{D}}). \quad (6)$$

Lemma 1 states that the marginal likelihood by model (1) can be written as a product of  $K$  multivariate normal densities, which simplifies the computation. In particular, instead

of computing the multivariate normal densities with a  $Kn \times Kn$  covariance matrix, one can evaluate the densities by  $K$  independent multivariate normal distributions, each of which has an  $n \times n$  covariance matrix. The direct computation of the inverse of an  $n \times n$  covariance matrix, however, is still very hard in general, when  $n$  is at the size of  $10^6$ . An efficient way that computes the exact likelihood will be provided in Section 3.

Denote  $\mathbf{Y}(s_j^*) = (\mathbf{y}(s_j^*)^T; \mathbf{y}^*(s_j^*)^T)^T$ , where  $\mathbf{y}(s_j^*)$  and  $\mathbf{y}^*(s_j^*)$  are the  $j^{\text{th}}$  column of  $\mathbf{y}(\mathbf{s}^*)$  and  $\mathbf{y}^*(\mathbf{s}^*)$  respectively. The goal of imputation is to find the predictive distribution at an unexamined site  $s_j^*$  conditioning on the available data, which is given in the lemma below.

**Lemma 2.** *We assume the same conditions in Lemma 1.*

1. For every  $s_j^*$ ,  $j = 1, \dots, n^*$ , denote  $\mathbf{r}_i(s_j^*) = (c_i(s_j^*, s_1^{\mathcal{D}}), \dots, c_i(s_j^*, s_n^{\mathcal{D}}))^T$ ,  $\mathbf{D}^*(s_j^*)$ . One has

$$\mathbf{Y}(s_j^*) \mid \mathbf{Y}(\mathbf{s}^{\mathcal{D}}), \sigma_0^2, \boldsymbol{\tau}_{1:K}^2, \boldsymbol{\gamma}_{1:K}, \boldsymbol{\eta}_{1:K} \sim MN\left(\hat{\boldsymbol{\mu}}(s_j^*), \hat{\boldsymbol{\Sigma}}(s_j^*)\right).$$

Here  $\hat{\boldsymbol{\mu}}(s_j^*) = \mathbf{A}\hat{\mathbf{v}}^*(s_j^*)$ , where the  $i^{\text{th}}$  entry of  $\hat{\mathbf{v}}^*(s_j^*)$  is  $\hat{v}_i^*(s_j^*) = \mathbf{r}_i^T(s_j^*)(\tilde{\mathbf{R}}_i + \frac{\sigma_0^2(\mathbf{a}_i^T \mathbf{a}_i)^{-1}}{\tau_i^2} \mathbf{I}_n)^{-1} \hat{\mathbf{v}}_i(\mathbf{s}^{\mathcal{D}})$  with  $\hat{\mathbf{v}}_i(\mathbf{s}^{\mathcal{D}})$  being the transpose of the  $i^{\text{th}}$  row of  $\hat{\mathbf{v}}(\mathbf{s}^{\mathcal{D}})$  defined in Equation (6), and  $\hat{\boldsymbol{\Sigma}}(s_j^*) = \mathbf{A}\mathbf{D}^*(s_j^*)\mathbf{A}^T + \sigma_0^2 \mathbf{I}_K$ , where  $\mathbf{D}^*(s_j^*)$  is a diagonal matrix with the  $i^{\text{th}}$  diagonal term being  $\tau_i^2(\tilde{c}_i(s_j^*, s_j^*) - \mathbf{r}_i^T(s_j^*)(\tilde{\mathbf{R}}_i + \frac{\sigma_0^2(\mathbf{a}_i^T \mathbf{a}_i)^{-1}}{\tau_i^2} \mathbf{I}_n)^{-1} \mathbf{r}_i(s_j^*))$ , for  $i = 1, \dots, K$ .

2. Denote the partition  $\hat{\boldsymbol{\mu}}(s_j^*) = (\hat{\boldsymbol{\mu}}_0^T(s_j^*), \hat{\boldsymbol{\mu}}_*^T(s_j^*))^T$  and  $\hat{\boldsymbol{\Sigma}}(s_j^*) = \begin{pmatrix} \hat{\boldsymbol{\Sigma}}_{00}(s_j^*) & \hat{\boldsymbol{\Sigma}}_{0*}(s_j^*) \\ \hat{\boldsymbol{\Sigma}}_{*0}(s_j^*) & \hat{\boldsymbol{\Sigma}}_{**}(s_j^*) \end{pmatrix}$ .

For every  $s_j^*$ , the predictive distribution of the unobserved  $\mathbf{y}^*(s_j^*)$  follows

$$\mathbf{y}^*(s_j^*) \mid \mathbf{y}(\mathbf{s}^{\mathcal{D}}), \mathbf{y}(\mathbf{s}^*), \mathbf{y}^*(\mathbf{s}^{\mathcal{D}}), \sigma_0^2, \boldsymbol{\tau}_{1:K}^2, \boldsymbol{\gamma}_{1:K}, \boldsymbol{\eta}_{1:K} \sim MN\left(\hat{\boldsymbol{\mu}}_{*|0}(s_j^*), \hat{\boldsymbol{\Sigma}}_{*|0}(s_j^*)\right),$$

where  $\hat{\boldsymbol{\mu}}_{*|0}(s_j^*) = \hat{\boldsymbol{\mu}}_*(s_j^*) + \hat{\boldsymbol{\Sigma}}_{*0}(s_j^*)\hat{\boldsymbol{\Sigma}}_{00}^{-1}(s_j^*)(\mathbf{y}(s_j^*) - \hat{\boldsymbol{\mu}}_0(s_j^*))$  and  $\hat{\boldsymbol{\Sigma}}_{*|0}(s_j^*) = \hat{\boldsymbol{\Sigma}}_{**}(s_j^*) - \hat{\boldsymbol{\Sigma}}_{*0}(s_j^*)\hat{\boldsymbol{\Sigma}}_{00}^{-1}(s_j^*)\hat{\boldsymbol{\Sigma}}_{0*}(s_j^*)$ .

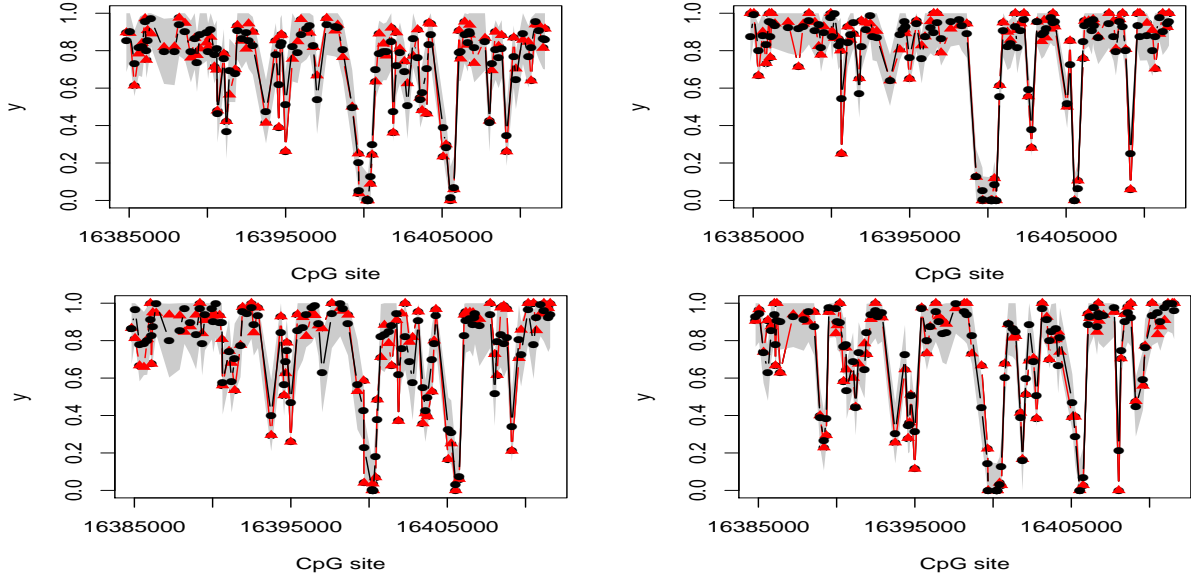


Figure 2: The held-out methylation levels (red triangles) and prediction of methylation levels (black dots) by the nonseparable GaSP model for randomly selected 4 samples at 100 CpG sites. The 95% posterior predictive interval is dashed as the shaded area. 25% of the observations at the first million CpG sites in chromosome 1 in the WGBS data of these 4 samples are held out for testing.

In the methylation levels imputation study,  $\hat{\mu}_{*|0}(s_j^*)$  can be used as predictions for  $\mathbf{y}^*(s_j^*)$  for any site  $s_j^*$ , by properly conditional on all observations. Note that the model and predictive distribution given in Lemma 1 and Lemma 2 are not identifiable between  $\eta_1, \dots, \eta_K$ , and  $\sigma_0^2$ . In the following, we simply constrain  $\sigma_0^2 = 0$  to avoid the potential identifiability issue.

Figure 2 plots the predicted methylation levels as the black dots at 100 held-out CpG sites for 4 samples in the WGBS data, and held out methylation levels are marked as the red triangles. The prediction by the nonseparable GaSP model captures the pattern of the methylation levels reasonably well, with an adequate length of 95% predictive interval, graphed as the shaded area. A more detailed comparison between the nonseparable GaSP model and other computational feasible alternatives is given in Section 5.

### 3 Computational strategy

The computations of the likelihood in model (1) require to compute the inverse of  $\mathbf{R}_i$ , each with  $O(n^3)$  operations, making the implementation impractical when  $n$  is large. We introduce a computationally efficient algorithm, based on the connection between the Gaussian random field and Gaussian Markov random field (GMRF) (Whittle, 1954, 1963). The idea was recently introduced in Hartikainen and Sarkka (2010). Unlike many other methods, no approximation to the likelihood is needed in this approach. We briefly review this computational strategy and extend it to compute the likelihood of the nonseparable GaSP model.

Consider a continuous auto-regressive model with order  $p$ , defined by a stochastic differential equation (SDE),

$$c_p v^{(p)}(s) + c_{p-1} v^{(p-1)}(s) + \dots + c_0 v(s) = b_0 z(s), \quad (7)$$

where  $v^{(l)}(s)$  is the  $l^{\text{th}}$  derivative of  $v(s)$  and  $z(s)$  is the standard Gaussian white noise process defined on  $s \in \mathbb{R}$ . Here we set  $c_p = 1$  to avoid the nonidentifiability issue. The spectral density of equation (7) is  $S_{\mathbb{R}}(t) = \frac{b_0^2}{|C(2\pi it)|^2}$ , where  $i$  is the imaginary number, and the operator  $C(\cdot)$  is defined by  $C(z) = \sum_{l=0}^p c_l z^l$ . The form of the above spectral density is  $S_{\mathbb{R}}(t) = \frac{\text{constant}}{\text{polynomial in } t^2}$ , which is a rational functional form. It has been shown in Whittle (1954, 1963) that the spectral density of GaSP with the Matérn covariance is

$$S_{Mat}(t) \propto \frac{1}{(\lambda^2 + t^2)^{(\nu+1/2)}}, \quad (8)$$

where  $\lambda = \frac{\sqrt{2\nu}}{\gamma}$  with the range parameter  $\gamma$  and the smoothness parameter  $\nu$ . The spectral density in (8) follows a rational functional form, meaning that we can utilize the GMRF representation for computation, elaborated in the following subsection.

### 3.1 The computation by continuous time stochastic process

As shown in Lemma 1, the likelihood of  $\mathbf{Y}(\mathbf{s}^{\mathcal{D}})$  in model (1) is proportional to  $K$  multivariate normal distribution at  $\hat{\mathbf{v}}_i(\mathbf{s}^{\mathcal{D}})$ , which is the transpose of the  $i$ th row of  $\hat{\mathbf{v}}(\mathbf{s}^{\mathcal{D}}) = (\mathbf{A}^T \mathbf{A})^{-1} \mathbf{A}^T \mathbf{Y}(\mathbf{s}^{\mathcal{D}})$ . We thus focus on  $\hat{\mathbf{v}}(\mathbf{s}^{\mathcal{D}})$  with  $\sigma_0^2 = 0$  due to the identifiability reason.

For demonstration purposes, we assume a Matérn kernel with  $\nu = 5/2$  for the latent factor processes

$$c(d) = \left( 1 + \frac{\sqrt{5}d}{\gamma} + \frac{5d^2}{3\gamma^2} \right) \exp \left( -\frac{\sqrt{5}d}{\gamma} \right), \quad (9)$$

with  $d = |s_a - s_b|$  for any  $s_a, s_b \in \mathcal{S}$ . The computational advantages introduced in this subsection hold for Matérn kernel with  $\nu = (2m + 1)/2$  for all  $m \in \mathbb{N}$ . One can also use the Matérn kernel with different smoothness parameter  $\nu_i$  for  $\hat{\mathbf{v}}_i(\mathbf{s}^{\mathcal{D}})$  to reflect the change of the smoothness in the trajectories of factor processes.

For any  $s \in \mathcal{S}$ , the nonseparable GaSP model in (1) can be represented as

$$\begin{aligned} \hat{v}_i(s) &= v_i(s) + \epsilon_i, \\ v_i(\cdot) &\sim \text{GaSP}(0, \tau_i^2 c_i(\cdot, \cdot)), \end{aligned} \quad (10)$$

where  $\epsilon_i \sim \text{N}(0, \sigma_i^2)$  being an independent noise. Denote  $\boldsymbol{\theta}_i(s) := (v_i(s), v_i^{(1)}(s), v_i^{(2)}(s))^T$ , where  $v_i^{(l)}(s)$  is the  $l^{\text{th}}$  derivative of  $v_i(s)$  with regard to  $s$ , for  $l = 1, 2$ . The GaSP model defined in (10) with the correlation in (9) follows an SDE:  $\frac{d\boldsymbol{\theta}_i(s)}{ds} = \mathbf{J}_i \boldsymbol{\theta}_i(s) + \mathbf{L} z_i(s)$ , where  $z_i(s)$  is a zero-mean Gaussian white noise process with variance  $\tau_i^2$  and  $\lambda_i = \sqrt{2\nu_i}/\gamma_i$ , for  $i = 1, \dots, K$ . The closed form expression of  $\mathbf{J}_i$  and  $\mathbf{L}$  is given in the supplementary materials.

Denote  $q_i = \frac{16}{3} \sigma_i^2 \lambda_i^5$  and  $\mathbf{F} = (1, 0, 0)$ . The solution of the SDE for model (10) can be

represented explicitly as follows (Hartikainen and Sarkka, 2010),

$$\begin{aligned}\hat{v}_i(s_{j+1}) &= \mathbf{F}\boldsymbol{\theta}_i(s_{j+1}) + \epsilon_i, \\ \boldsymbol{\theta}_i(s_{j+1}) &= \mathbf{G}_i(s_j)\boldsymbol{\theta}_i(s_j) + \mathbf{w}_i(s_j),\end{aligned}\tag{11}$$

where  $\mathbf{w}_i(s_j) \sim \text{MN}(\mathbf{0}, \mathbf{W}_i(s_j))$  with  $\mathbf{G}_i(s_j) = e^{\mathbf{J}_i(s_{j+1}-s_j)}$  and  $\mathbf{W}_i(s_j) = \int_0^{s_{j+1}-s_j} e^{\mathbf{J}_i t} \mathbf{L} q_i \mathbf{L}^T e^{\mathbf{J}_i^T t} dt$  for  $i = 1, \dots, K$  and  $j = 1, \dots, N-1$ . The stationary distribution at  $\boldsymbol{\theta}_i$  is  $\boldsymbol{\theta}_i(s_0) \sim \text{MN}(\mathbf{0}, \mathbf{W}_i(s_0))$ , with  $\mathbf{W}_i(s_0) = \int_0^\infty e^{\mathbf{J}_i t} \mathbf{L} q_i \mathbf{L}^T e^{\mathbf{J}_i^T t} dt$ . All  $\mathbf{G}_i(s_j)$ ,  $\mathbf{W}_i(s_j)$ ,  $\mathbf{W}_i(s_0)$ , and the likelihood of  $\boldsymbol{\theta}_i$  are given in the supplementary materials.

The following Lemma 3 is the Kalman filter for the continuous state space model in (11) (see e.g. Chapter 4 in West and Harrison (1997) and Chapter 2 in Petris et al. (2009)).

**Lemma 3** (Kalman filter). *Consider the continuous time state space model specified by Equation (11). To simplify the denotation, we assume all the distributions in this lemma are conditional on the parameters  $(\sigma_i^2, \tau_i^2, \gamma_i)$ . For each  $i = 1, \dots, K$ , denote*

$$\boldsymbol{\theta}_i(s_{j-1}^{\mathcal{D}}) \mid \hat{\mathbf{v}}_i(\mathbf{s}_{1:j-1}^{\mathcal{D}}) \sim \text{MN}(\mathbf{m}_i(s_{j-1}^{\mathcal{D}}), \mathbf{C}_i(s_{j-1}^{\mathcal{D}})),$$

for any  $j \geq 1$  (where  $s_0^{\mathcal{D}}$  is defined to be an empty set, meaning that we don't condition on any observation when  $j = 1$ ). One has the following statements for each  $i = 1, \dots, K$ .

(i) *The one-step-ahead predictive distribution of  $\boldsymbol{\theta}_i(s_j^{\mathcal{D}})$  given  $\hat{\mathbf{v}}_i(\mathbf{s}_{1:j-1}^{\mathcal{D}})$  is*

$$\boldsymbol{\theta}_i(s_j^{\mathcal{D}}) \mid \hat{\mathbf{v}}_i(\mathbf{s}_{1:j-1}^{\mathcal{D}}) \sim \text{MN}(\boldsymbol{\mu}_{\boldsymbol{\theta}_i}(s_j^{\mathcal{D}}), \boldsymbol{\Sigma}_{\boldsymbol{\theta}_i}(s_j^{\mathcal{D}})),\tag{12}$$

where  $\boldsymbol{\mu}_{\boldsymbol{\theta}_i}(s_j^{\mathcal{D}}) = \text{E}[\boldsymbol{\theta}_i(s_j^{\mathcal{D}}) \mid \hat{\mathbf{v}}_i(\mathbf{s}_{1:j-1}^{\mathcal{D}})] = \mathbf{G}_i(s_j^{\mathcal{D}})\mathbf{m}_i(s_{j-1}^{\mathcal{D}})$  and  $\boldsymbol{\Sigma}_{\boldsymbol{\theta}_i}(s_j^{\mathcal{D}}) = \text{Var}[\boldsymbol{\theta}_i(s_j^{\mathcal{D}}) \mid \hat{\mathbf{v}}_i(\mathbf{s}_{1:j-1}^{\mathcal{D}})] = \mathbf{G}_i(s_j^{\mathcal{D}})\mathbf{C}_i(s_{j-1}^{\mathcal{D}})\mathbf{G}_i^T(s_j^{\mathcal{D}}) + \mathbf{W}_i(s_j^{\mathcal{D}})$ .

(ii) The one-step-ahead predictive distribution of  $\hat{v}_i(s_j^{\mathcal{D}})$  given  $\hat{\mathbf{v}}_i(\mathbf{s}_{1:j-1}^{\mathcal{D}})$  is

$$\hat{v}_i(s_j^{\mathcal{D}}) \mid \hat{\mathbf{v}}_i(\mathbf{s}_{1:j-1}^{\mathcal{D}}) \sim N(f_i(s_j^{\mathcal{D}}), Q_i(s_j^{\mathcal{D}})), \quad (13)$$

where  $f_i(s_j^{\mathcal{D}}) = \mathbb{E}[\hat{v}_i(s_j^{\mathcal{D}}) \mid \hat{\mathbf{v}}_i(\mathbf{s}_{1:j-1}^{\mathcal{D}})] = \mathbf{F}\boldsymbol{\mu}_{\theta_i}(s_j^{\mathcal{D}})$  and  $Q_i(s_j^{\mathcal{D}}) = \text{Var}[\hat{v}_i(s_j^{\mathcal{D}}) \mid \hat{\mathbf{v}}_i(\mathbf{s}_{1:j-1}^{\mathcal{D}})] = \mathbf{F}\boldsymbol{\Sigma}_{\theta_i}(s_j^{\mathcal{D}})\mathbf{F}^T + \sigma_i^2$ .

(iii) The filtering distribution of  $\boldsymbol{\theta}_i(s_j^{\mathcal{D}})$  given  $\hat{\mathbf{v}}_i(\mathbf{s}_{1:j}^{\mathcal{D}})$  is

$$\boldsymbol{\theta}_i(s_j^{\mathcal{D}}) \mid \hat{\mathbf{v}}_i(\mathbf{s}_{1:j}^{\mathcal{D}}) \sim MN(\mathbf{m}_i(s_j^{\mathcal{D}}), \mathbf{C}_i(s_j^{\mathcal{D}})), \quad (14)$$

where  $\mathbf{m}_i(s_j^{\mathcal{D}}) = \mathbb{E}[\boldsymbol{\theta}_i(s_j^{\mathcal{D}}) \mid \hat{\mathbf{v}}_i(\mathbf{s}_{1:j}^{\mathcal{D}})] = \boldsymbol{\mu}_{\theta_i}(s_j^{\mathcal{D}}) + \boldsymbol{\Sigma}_{\theta_i}(s_j^{\mathcal{D}})\mathbf{F}^T Q_i^{-1}(s_j^{\mathcal{D}}) e_i(s_j^{\mathcal{D}})$  and  $\mathbf{C}_i(s_j^{\mathcal{D}}) = \text{Var}[\boldsymbol{\theta}_i(s_j^{\mathcal{D}}) \mid \hat{\mathbf{v}}_i(\mathbf{s}_{1:j}^{\mathcal{D}})] = \boldsymbol{\Sigma}_{\theta_i}(s_j^{\mathcal{D}}) - \boldsymbol{\Sigma}_{\theta_i}(s_j^{\mathcal{D}})\mathbf{F}^T Q_i^{-1}(s_j^{\mathcal{D}})\mathbf{F}\boldsymbol{\Sigma}_{\theta_i}(s_j^{\mathcal{D}})$ , with  $e_i(s_j^{\mathcal{D}}) = \hat{v}_i(s_j^{\mathcal{D}}) - f_i(s_j^{\mathcal{D}})$  being the forecast error.

For the purpose of computing the likelihood discussed in the next subsection, we define the Kalman filter on  $\mathbf{s}^{\mathcal{D}}$  in Lemma 3. Given an estimate of  $(\sigma_i^2, \tau_i^2, \gamma_i)$  for  $i = 1, \dots, K$ , we implement the Kalman filter for all sites  $\mathbf{s}_{1:N}$ , which includes  $\mathbf{s}^*$ . Filtering sites without an observation can be done in Kalman filter in Lemma 3 and we refer the reader to Section 2.7.3. in Petris et al. (2009) for the details. The following Kalman smoother provides the predictive distribution for all sites  $\mathbf{s}_{1:N}$  (see West and Harrison (1997) and Petris et al. (2009)).

**Lemma 4** (Kalman smoother). *Consider the continuous time state space model specified by Equation (11). We assume all the distributions in this lemma are conditional on  $(\sigma_i^2, \tau_i^2, \gamma_i)$ . For  $i = 1, \dots, K$  and  $j = 1, \dots, N - 1$ , let  $\boldsymbol{\theta}_i(s_{j+1}) \mid \hat{\mathbf{v}}_i(\mathbf{s}^{\mathcal{D}}) \sim N(\boldsymbol{\mu}_{\theta_i}^*(s_{j+1}), \boldsymbol{\Sigma}_{\theta_i}^*(s_{j+1}))$ , then*

$$\boldsymbol{\theta}_i(s_j) \mid \hat{\mathbf{v}}_i(\mathbf{s}^{\mathcal{D}}) \sim MN(\boldsymbol{\mu}_{\theta_i}^*(s_j), \boldsymbol{\Sigma}_{\theta_i}^*(s_j)),$$

where  $\boldsymbol{\mu}_{\theta_i}^*(s_j) = \mathbf{m}_i(s_j) + \mathbf{C}_i(s_j)\mathbf{G}_i^T(s_{j+1})\boldsymbol{\Sigma}_{\theta_i}^{-1}(s_{j+1})(\boldsymbol{\mu}_{\theta_i}^*(s_{j+1}) - \boldsymbol{\mu}_{\theta_i}(s_{j+1}))$  and  $\boldsymbol{\Sigma}_{\theta_i}^*(s_j) =$

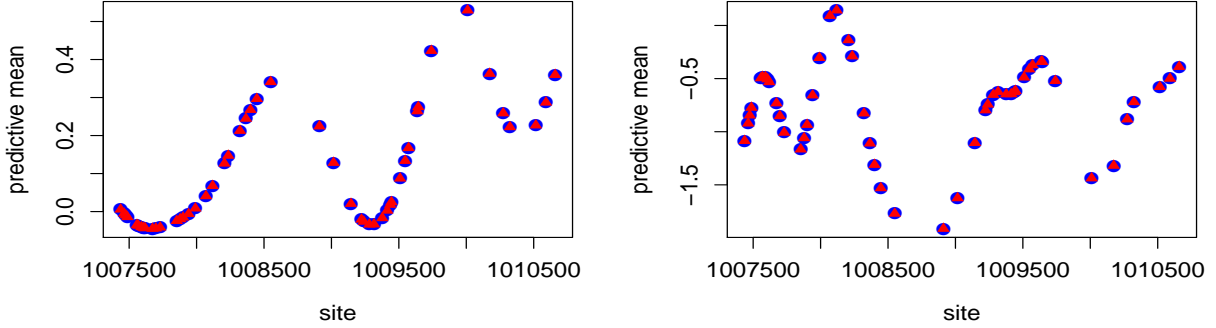


Figure 3: Predictive mean from the direct inversion of the covariance and from the FFBS algorithm. The blue dots are  $\hat{\mathbf{v}}_i(\mathbf{s}_{1:50}^*)|\hat{\mathbf{v}}_i(\mathbf{s}_{1:400}^{\mathcal{D}})$  computed by equation (11) for  $i = 1$  (left panel) and  $i = 2$  (right panel), for a given set of parameters  $(\sigma_i^2, \gamma_i, \tau_i)$ . The red triangles (overlapping the blue dots) are the same quantities by the direct computation for the GaSP model. The root of mean square errors (RMSE) between the blue dots and red triangles at these 50 sites are  $8.86 \times 10^{-30}$  and  $2.05 \times 10^{-30}$  for the left panel and right panel, respectively.

$$\mathbf{C}_i(s_j) - \mathbf{C}_i(s_j)\mathbf{G}_i^T(s_{j+1})\boldsymbol{\Sigma}_{\boldsymbol{\theta}_i}^{-1}(s_{j+1})(\boldsymbol{\Sigma}_{\boldsymbol{\theta}_i}(s_{j+1}) - \boldsymbol{\Sigma}_{\boldsymbol{\theta}_i}^*(s_{j+1}))\boldsymbol{\Sigma}_{\boldsymbol{\theta}_i}^{-1}(s_{j+1})\mathbf{G}_i(s_{j+1})\mathbf{C}_i(s_j).$$

With the above setup, the posterior for  $\boldsymbol{\theta}_i(s)$ ,  $i = 1, \dots, K$ , can be computed by a forward filtering and backward smoothing (FFBS) algorithm (West and Harrison, 1997), which only requires  $O(n)$  computational operations, a lot smaller than  $O(n^3)$  operations in the direct computation of the GaSP model. The prediction at  $\mathbf{s}^*$  also only requires linear computational operations to the number of sites, so the total computational operations are only  $O(N)$  altogether. The fast algorithm of evaluating the likelihood and making prediction is implemented in an R package on CRAN (Gu, 2019a).

Figure 3 compares the posterior mean at some site  $s_j^*$  by the FFBS algorithm and direct computation of GaSP for a given set of parameters. Since they are the same quantities computed in two different ways, the difference is extremely small. The main advantage of our method is that all summary statistics of interest, such as the posterior predictive mean and variance, as well as the marginal likelihood can be computed exactly.

The computational time between the algorithms, however, differs significantly. As shown



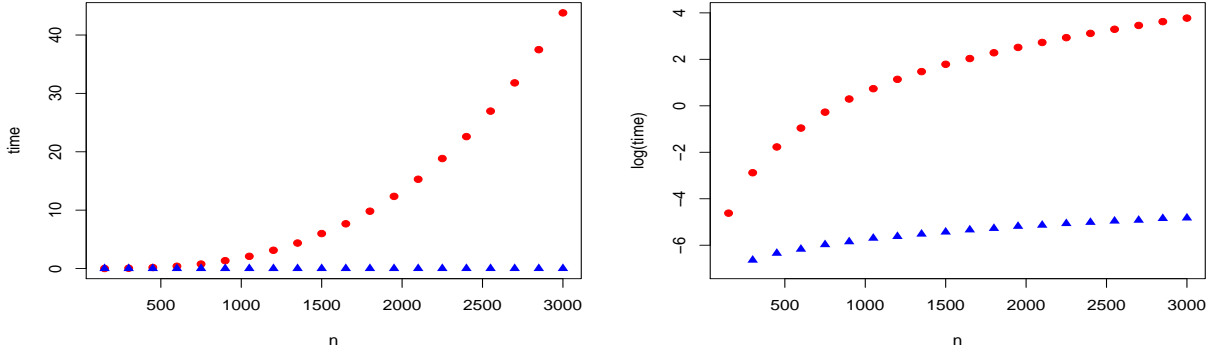


Figure 4: Computational time in seconds for one evaluation of the likelihood in seconds (left panel) and in natural logarithm of seconds (right panel). The red dot represents the computational time by the direct computation and blue solid triangle is by the FFBS algorithm.

in Figure 4, the computation by the FFBS algorithm is a lot more efficient than the direct evaluation of the likelihood, which requires  $O(n^3)$  for matrix inversion. For instance, when  $n = 3,000$ , evaluating the likelihood by the FFBS algorithm takes less than 0.01 second, while the direct computation takes more than 40 seconds in R.

Note when  $\nu_i = 5/2$ , the Matérn covariance matrix in (9) and its inversion are both dense  $n \times n$  matrices with rank  $n$ . However, the covariance matrix of the latent states,  $\theta_i(s) = (v_i(s), v_i^{(1)}(s), v_i^{(2)}(s))^T$  is sparse, as shown in supplementary materials. The result holds for all Matérn classes when  $\nu_i = (2m + 1)/2$ , with  $m \in \mathbb{N}$ .

### 3.2 Parameter estimation

The most computationally intensive part of the FFBS algorithm discussed in Section 3.1 is to sample the latent states. Fortunately, one can marginalize out the latent states explicitly,

$$p(\hat{\mathbf{v}}(\mathbf{s}^{\mathcal{D}}) | \sigma_{1:K}^2, \tau_{1:K}^2, \gamma_{1:K}) = \prod_{i=1}^K \left\{ p(\hat{v}_i(s_1^{\mathcal{D}}) | \sigma_i^2, \tau_i^2, \gamma_i) \prod_{j=2}^n p(\hat{v}_i(s_j^{\mathcal{D}}) | \hat{v}_i(\mathbf{s}_{1:j-1}^{\mathcal{D}}), \sigma_i^2, \tau_i^2, \gamma_i) \right\},$$

each term of which follows a normal distribution given in the one-step look ahead prediction in the FFBS algorithm (West and Harrison, 1997). The Lemma 5 below show that the marginal likelihood can be computed with  $O(n)$  computational operations.

**Lemma 5** (Likelihood by the Kalman filter). *For each  $i = 1, \dots, K$ , one has*

$$p(\hat{\mathbf{v}}_i(\mathbf{s}_{1:j}^{\mathcal{S}}) \mid \sigma_i^2, \tau_i^2, \gamma_i) = (2\pi)^{-n/2} \prod_{j=1}^n Q_i^{-1/2}(s_j^{\mathcal{S}}) \exp \left\{ - \sum_{j=1}^n \frac{(\hat{v}_i(s_j^{\mathcal{S}}) - f_i(s_j^{\mathcal{S}}))^2}{Q_i(s_j^{\mathcal{S}})} \right\}, \quad (15)$$

where  $f_i(s_j^{\mathcal{S}})$  and  $Q_i(s_j^{\mathcal{S}})$  are given in Lemma 3.

Lemma 5 is a direct consequence of the step (ii) in Lemma 3 so the proof is omitted here. To complete the model, we assume the prior as follows,

$$\pi(\boldsymbol{\sigma}_{1:K}^2, \boldsymbol{\tau}_{1:K}^2, \boldsymbol{\gamma}_{1:K}) \propto \prod_{i=1}^K \frac{\pi(\tau_i^2, \gamma_i)}{\sigma_i^2}. \quad (16)$$

Denote  $\zeta_i := 1/\gamma_i$  and  $\eta_i := \tau_i/\sigma_i^2$ . We assume the jointly robust prior (Gu, 2019b) for the transformed parameters  $\pi(\zeta_i, \eta_i) \propto (C_i \zeta_i + \eta_i)^{a_i} \exp(-b_i(C_i \zeta_i + \eta_i))$ , for  $i = 1, \dots, K$ , where  $C_i$ ,  $a_i$  and  $b_i$  are prior parameters. This prior approximates the reference prior in tail rates and is robust for posterior mode estimation (Gu et al., 2018). For the prior parameter, we use the default choice  $a = 1/2$ ,  $b = 1$ , and  $C_i = |\mathcal{S}|/n$ , where  $|\mathcal{S}|$  is the length of  $\mathcal{S}$ .

As  $n$  is large, the Markov chain Monte Carlo (MCMC) algorithm is still very slow for sampling the posterior distribution. We estimate the parameters by the posterior mode,

$$(\hat{\zeta}_i, \hat{\eta}_i) = \underset{\zeta_i, \eta_i}{\operatorname{argmax}} \{ p(\hat{\mathbf{v}}(\mathbf{s}^{\mathcal{S}}) \mid \zeta_i, \eta_i) \pi(\zeta_i, \eta_i) \}. \quad (17)$$

We summarize the estimation and prediction in the nonseparable GaSP model in Algorithm 1. We assume the mean of each row of the observations were subtracted before the estimation and added back for predictions.

---

**Algorithm 1** Estimation and prediction by the nonseparable GaSP model

---

- (1) Calculate  $\mathbf{A} = \mathbf{U}\mathbf{D}/\sqrt{n}$ , where  $\mathbf{U}$  and  $\mathbf{D}$  are from the SVD of  $\mathbf{Y}(\mathbf{s}^{\mathcal{D}})$ .
  - (2) Compute  $\hat{\mathbf{v}}(\mathbf{s}^{\mathcal{D}}) = (\mathbf{A}^T \mathbf{A})^{-1} \mathbf{A}^T \mathbf{Y}(\mathbf{s}^{\mathcal{D}})$ .
  - (3) Estimate the parameters by maximizing the posterior distribution in Equation (17), where the likelihood is calculated by Equation (15).
  - (4) Plugging the estimates  $(\hat{\sigma}_i^2, \hat{\tau}_i^2, \hat{\gamma}_i)$  for  $i = 1, \dots, K$  and implement the Kalman filter algorithm on all sites  $\mathbf{s}_{1:N}$  using Lemma 5. The output is the predictive mean and predictive variance of  $\hat{\mathbf{v}}_i(\mathbf{x}_j^*) \mid \hat{\mathbf{v}}_i(\mathbf{x}^{\mathcal{D}})$  for  $j = 1, \dots, n^*$ .
  - (5) Produce the predictive distribution using Lemma 2.
- 

## 4 Model unification

In this section, we show the linear regression that was used for methylation level imputation (Zhang et al., 2015), and the separable GaSP model used in computer model emulation (Conti and O’Hagan (2010); Gu and Berger (2016)) are both special cases of the nonseparable GaSP model introduced in Section 2.

### 4.1 Linear regression

Assuming that the samples are independent to each other, a simple model is to apply the linear regression separately for each CpG site  $s_j$ ,  $j = 1, \dots, N$ , as follows,

$$y_i(s_j) = \mathbf{H}_i(s_j)\boldsymbol{\beta}_j + \epsilon_{ij}, \quad i = 1, \dots, K, \quad (18)$$

where  $\mathbf{H}_i(s_j)$  are the covariates for the  $j^{\text{th}}$  CpG site of the  $i^{\text{th}}$  sample and  $\epsilon_{ij} \sim N(0, \sigma_{0j}^2)$  is an independent mean-zero Gaussian noise. In Zhang et al. (2015), some site-specific features, such as methylation levels at nearby CpG sites, are used as covariates for imputation. This approach assumes that methylation levels are independent across samples at every CpG site. However, methylation levels of different samples at a CpG site are generally correlated, as shown in Figure 1. Numerical results will be shown that exploiting the correlation between samples leads to drastic improvement in imputation in Section 5.

Alternatively, a regression model that exploits the correlations across samples follows

$$y_i^*(s_j) = \mathbf{H}_i(s_j)\boldsymbol{\beta}_i + \epsilon_{ij}, j = 1, \dots, N, \quad (19)$$

with  $\epsilon_{ij} \sim N(0, \sigma_{i0}^2)$ . Here each site is treated independently. Assume the methylation levels were first centered to have a zero mean and let  $\mathbf{H}_i(s_j) = (y_1(s_j), \dots, y_k(s_j))$ , meaning only the methylation levels of the  $k$  samples with full observations are used as covariates, the model for  $\mathbf{s}^{\mathcal{D}}$  can be expressed  $\mathbf{y}_i^*(\mathbf{s}^{\mathcal{D}})^T = \mathbf{y}(\mathbf{s}^{\mathcal{D}})^T \boldsymbol{\beta}_i + \epsilon_i$ , where  $\mathbf{y}_i^*(\mathbf{s}^{\mathcal{D}})$  is the  $i^{\text{th}}$  row of  $\mathbf{y}^*(\mathbf{s}^{\mathcal{D}})$  and  $\epsilon_i \sim \text{MN}(\mathbf{0}, \sigma_{i0}^2 \mathbf{I}_n)$ . The least squares (LS) estimator of  $\boldsymbol{\beta}_i$  is  $\hat{\boldsymbol{\beta}}_i = \{\mathbf{y}(\mathbf{s}^{\mathcal{D}})\mathbf{y}(\mathbf{s}^{\mathcal{D}})^T\}^{-1} \mathbf{y}(\mathbf{s}^{\mathcal{D}})\mathbf{y}_i^*(\mathbf{s}^{\mathcal{D}})^T$ , where  $\mathbf{y}_i^*(\mathbf{s}^{\mathcal{D}}) = (y_i^*(\mathbf{s}_1^{\mathcal{D}}), \dots, y_i^*(\mathbf{s}_n^{\mathcal{D}}))$  being the  $i^{\text{th}}$  row of  $\mathbf{y}^*(\mathbf{s}^{\mathcal{D}})$ . The predictive mean of the methylation level of the  $i^{\text{th}}$  sample at the  $j^{\text{th}}$  unexamined site,  $\mathbf{H}_i(s_j^*)\hat{\boldsymbol{\beta}}_i$ , follows

$$\text{E}[\mathbf{y}_i^*(s_j^*) \mid \mathbf{y}(\mathbf{s}^{\mathcal{D}}), \mathbf{y}^*(\mathbf{s}^{\mathcal{D}}), \mathbf{y}(\mathbf{s}^*), \hat{\boldsymbol{\beta}}_i] = \mathbf{y}(s_j^*)^T \{\mathbf{y}(\mathbf{s}^{\mathcal{D}})\mathbf{y}(\mathbf{s}^{\mathcal{D}})^T\}^{-1} \mathbf{y}(\mathbf{s}^{\mathcal{D}})\mathbf{y}_i^*(\mathbf{s}^{\mathcal{D}})^T, \quad (20)$$

with  $\mathbf{y}(s_j^*) = (y_1(s_j^*), \dots, y_k(s_j^*))^T$  being the  $j^{\text{th}}$  column of  $\mathbf{y}(\mathbf{s}^*)$ , for  $i = 1, \dots, k^*$ ,  $j = 1, \dots, n^*$ .

The following remark establish the connection between the linear regression and nonseparable GaSP model.

**Remark 1.** *The predictive mean under the linear regression model in (20) is identical to the predictive mean  $\hat{\boldsymbol{\mu}}_{*|0}(s_j^*)$  of the nonseparable model with  $\sigma_0^2 = 0$  in Lemma 2 if in model (1),*

(i.)  $\mathbf{A} = \mathbf{U}\mathbf{D}/\sqrt{n}$ , where  $\mathbf{U}$  and  $\mathbf{D}$  are defined through the SVD of  $\mathbf{Y}(\mathbf{s}^{\mathcal{D}})$ .

(ii.)  $\tilde{v}_i(\cdot)$  is the realization of independent mean zero Gaussian noise with the same variance.

## 4.2 Separable model

Denote  $\mathbf{Y}$  as a  $K \times N$  matrix where each row is a sample of methylation levels at  $N$  CpG sites. One may model the data through a joint model below

$$\mathbf{Y} = \mathbf{Z} + \boldsymbol{\epsilon}_0, \quad (21)$$

where  $\boldsymbol{\epsilon}_0$  is a zero-mean independent noise and  $\mathbf{Z}$  is a  $K \times N$  random matrix modeled from a matrix-variate normal distribution,  $\mathbf{Z} \sim N_{K,N}(\boldsymbol{\mu}, \boldsymbol{\Sigma}, \mathbf{R})$ , with a  $K \times N$  mean matrix  $\boldsymbol{\mu}$ , a  $K \times K$  row covariance matrix  $\boldsymbol{\Sigma}$ , and an  $N \times N$  column correlation matrix  $\mathbf{R}$ .

We call model (21) *the separable model*, as the correlations across samples and across sites are expressed separately by  $\boldsymbol{\Sigma}$  and  $\mathbf{R}$  respectively. Assuming that  $\Lambda$  is modeled by a correlation function, where the  $(i, j)$  entry  $\mathbf{R}_{i,j} = c(d)$ , with  $c(\cdot)$  being the correlation function. The following remark states the separable model defined in (21) is a special case of the nonseparable model in (1).

**Remark 2.** *Assuming  $\boldsymbol{\mu} = \mathbf{0}$ , the separable model defined in (21) is equivalent to the non-separable GaSP model in (1) if*

(i.)  $\mathbf{A}$  is chosen such that  $\boldsymbol{\Sigma} = \mathbf{A}\mathbf{A}^T$ .

(ii.) The covariance in (2) has a unit variance,  $c_i(d) = c(d)$ ,  $\eta_i = 0$ , for  $i = 1, \dots, K$ .

## 5 Numerical comparison

We evaluate the nonseparable GaSP model in (1) and compare to several alternative methods: two linear regression strategies (by site in (18) and by sample in (19)), nearest neighbor method (using only the observed methylation level closest to the unobserved site for prediction) and two regression strategies by the random forest algorithm (Breiman, 2001; Liaw and Wiener, 2002). We also introduce a localized Kriging method by partitioning the data

into small blocks, and compare it with the nonseparable GaSP model in the supplementary materials.

The performance of these methods is evaluated on the out of sample prediction for WGBS data and Methylation450K data available in (Ziller et al., 2013) and (Zhang et al., 2015), respectively. We focus on the following criteria:

$$\begin{aligned}
 RMSE &= \sqrt{\frac{\sum_{i=1}^{k^*} \sum_{j=1}^{n^*} (\hat{y}_i^*(s_j^*) - y_i^*(s_j^*))^2}{k^*n^*}}, \\
 P_{CI}(95\%) &= \frac{1}{k^*n^*} \sum_{i=1}^{k^*} \sum_{j=1}^{n^*} 1\{y_i^*(s_j^*) \in CI_{ij}(95\%)\}, \\
 L_{CI}(95\%) &= \frac{1}{k^*n^*} \sum_{i=1}^{k^*} \sum_{j=1}^{n^*} \text{length}\{CI_{ij}(95\%)\},
 \end{aligned}$$

where for  $1 \leq i \leq k^*$  and  $1 \leq j \leq n^*$ ,  $y_i^*(s_j^*)$  is the held-out methylation levels of the  $i^{th}$  sample at the  $j^{th}$  CpG site;  $\hat{y}_i^*(s_j^*)$  is the predicted held-out methylation level of the  $i^{th}$  sample at the  $j^{th}$  CpG site;  $CI_{ij}(95\%)$  is the 95% posterior credible interval; and  $\text{length}\{CI_{ij}(95\%)\}$  is the length of the 95% posterior credible interval. An effective method is expected to have small out-of-sample RMSE,  $P_{CI}(95\%)$  being close to nominal 95% level, and small  $L_{CI}(95\%)$ . In Zhang et al. (2015), a CpG site is defined to be methylated if more than 50% of the probes are methylated, and the accuracy of a method is defined by the proportion of the correct predictions of CpG sites being methylated or not. We also include the rate of accuracy as a criterion for comparison.

## 5.1 Application 1: WGBS data

We first compare the out-of-sample prediction of different methods using the criteria discussed above for  $10^6$  methylation levels at chromosome 1 in the WGBS dataset (Ziller et al., 2013). In this dataset, 24 samples are available in total and we randomly sample  $k^* = 4$  samples, whose methylation levels are partially observed (with certain proportion being held

out), while the methylation levels of the rest of the samples are fully observed. We consider three scenarios, in which 25%, 50%, 75%, and 90% of the methylation levels of these 4 samples are held out as the test dataset. The methylation levels of each sample are centered and the mean is added back for prediction in the GaSP model (Higdon et al., 2008). We estimate the range and nugget parameters using equation (17) and rely on the predictive distribution of model (1) for combining different sources of information in prediction.

As shown in Table 1, the nonseparable GaSP model has the smallest out-of-sample RMSE in out-of-sample prediction in almost all scenarios. For instance, when 50% of CpG sites are held out, the nonseparable GaSP method improves the RMSE by around 15% compared to any other methods we considered. The gain is from integrating the correlations between CpG sites and between samples through a coherent statistical model, while the other models only utilize partial information. For example, the methods in rows 2 to 4 only exploit the site-wise correlation by assuming the independence across different samples at each CpG site, while the methods in rows 5 to 6 only exploit the correlation between samples.

When more and more data are held-out as the test data, the correlation between nearby observed methylation levels gets smaller as the average distance between two sites with observed methylation levels gets larger, making it harder for prediction. We noticed the RMSE by the nonseparable GaSP model increases by more than 10% when the percentage of held-out site increases from 75% to 90%. In this scenario, the nonseparable GaSP model performs similar to the methods based on the sample correlation, and much better than the recent interpolation method based on the correlation between site (Zhang et al., 2015).

The nonseparable GaSP also leads to around 97% accuracy in predicting whether a CpG site is methylated or not, which is also the highest compared to all other methods. Note the differences between the nonseparable model and other methods are small, as around 90% of the CpG sites are methylated in this dataset, and thus a benchmark estimator could achieve at least 90% accuracy in prediction.

25% held-out CpG sites	RMSE	$P_{CI}(95\%)$	$L_{CI}(95\%)$	Accuracy
Nonseparable GaSP	.0835	.941	.258	.972
Nearest neighbor	.152	/	/	.942
Linear model by site	.0993	.912	.261	.966
Random forest by site	.103	/	/	.964
Linear model by sample	.100	.941	.308	.962
Random forest by sample	.0961	/	/	.965
50% held-out CpG sites	RMSE	$P_{CI}(95\%)$	$L_{CI}(95\%)$	Accuracy
Nonseparable GaSP	.0840	.943	.264	.971
Nearest neighbor	.153	/	/	.942
Linear model by site	.0993	.913	.262	.966
Random forest by site	.103	/	/	.964
Linear model by sample	.100	.941	.307	.962
Random forest by sample	.0965	/	/	.964
75% held-out CpG sites	RMSE	$P_{CI}(95\%)$	$L_{CI}(95\%)$	Accuracy
Nonseparable GaSP	.0887	.939	.271	.969
Nearest neighbor	.166	/	/	.934
Linear model by site	.106	.910	.274	.963
Random forest by site	.108	/	/	.962
Linear model by sample	.100	.940	.308	.962
Random forest by sample	.0972	/	/	.964
90% held-out CpG sites	RMSE	$P_{CI}(95\%)$	$L_{CI}(95\%)$	Accuracy
Nonseparable GaSP	.0984	.917	.267	.965
Nearest neighbor	.188	/	/	.922
Linear model by site	.114	.908	.289	.959
Random forest by site	.114	/	/	.958
Linear model by sample	.100	.941	.308	.962
Random forest by sample	.0983	/	/	.963

Table 1: Comparison of different methods for  $10^6$  methylation levels at chromosome 1 in the WGBS data. From the upper to the lower, 25%, 50%, 75% and 90% of the first million methylation levels of  $k^* = 4$  samples are held out for testing, respectively.

## 5.2 Application 2: Methylation450K data

In this section, we study the numerical performance of all the methods for all chromosomes the Methylation450K dataset (Zhang et al., 2015). In this dataset, the methylation levels at all chromosomes of 100 samples are recorded, which contains 2% methylation levels in the WGBS whole sequencing dataset. Our ultimate goal is to interpolate the methylation levels



	RMSE	$P_{CI}(95\%)$	$L_{CI}(95\%)$	Accuracy
Nonseparable GaSP	.0296	.958	.103	.991
Nearest neighbor	.350	/	/	.774
Linear model by site	.0342	.944	.099	.990
Random forest by site	.0339	/	/	.989
Linear model by sample	.0304	.957	.106	.990
Random forest by sample	.0304	/	/	.989

Table 2: Predictive performance of different approaches for the Methylation450K data.

at all chromosomes based on the Methylation450K dataset, so this dataset may give us a better sense of the performance of different approaches, compared to interpolation results at chromosome 1 using the WGBS whole sequencing dataset shown in Section 5.1.

The methylation levels at  $n^* = 7.4 \times 10^4$  CpG sites from  $k^* = 50$  samples are held out as the testing output, which is around 20% of the total CpG sites in the Methylation450K dataset. We do not hold out more CpG sites because the observations in the Methylation450K dataset is already very sparse. In Table 2, the prediction based on the nonseparable GaSP model has the lowest RMSE, and around 95% of the held-out data are covered in the 95% predictive interval. Furthermore, around half of the probes are methylated in this dataset on average, so the predictive accuracy of the nonseparable GaSP is high compared with a benchmark estimator.

Note that the CpG sites are sparse in the Methylation450K dataset, so the correlation of the methylation levels between nearby sites is smaller than the ones in the WGBS data. However, the long-ranged site-wise correlation is still useful for prediction. We found that the nearest neighbor method is the worst method among all, as it only employs the correlation at the nearest neighbor. The linear model by site and random forest by site employ the correlation on more neighboring sites, which improve the predictive accuracy. The nonseparable GaSP models both the correlation of the methylation levels between all sites and between all samples, leading to the most accurate predictions among the methods we compared.

The computation of the nonseparable GaSP model relies heavily on the fast and exact computation algorithm discussed in Section 3. Since the number of methylation levels is at the size of a million in one chromosome in one sample, direct computation of the GaSP model is infeasible. In the supplemental materials, we also compare with a localized Kriging method. The performance of the nonseparable GaSP model is still better, partly because the correlation between CpG sites is long-ranged, shown in the left panel of Figure 1.

## 6 Concluding remarks

This paper discusses modeling multiple functional data through Gaussian stochastic processes. We unify several different models, including the linear regression model and separable model, through a nonseparable GaSP framework. A computationally efficient algorithm is provided for the large scale problems without approximation to the likelihood. Several interesting future topics are worth exploring from both the computational and modeling perspectives. The achievement in computation is limited, in a sense that the input of the GaSP model (CpG site) is only 1 dimensional. It remains to be an issue to generalize this computational method for the case with multi-dimensional inputs. Some recent progresses of this direction are introduced in Lindgren et al. (2011), where the GaSP with a Matérn covariance can be represented by stochastic partial differential equations, while a method that computes the exact likelihood is still unknown. Furthermore, the outcomes of methylation levels are  $[0, 1]$  with lots of 0 and 1 in the dataset. One may model a point process with probability masses at 0 and 1 to further improve the accuracy in prediction.

In this work, we estimate the factor loadings by the principal component analysis. Another data-dependent way to estimate the factor loadings is by the generalized probabilistic principal component analysis (Gu and Shen, 2018), where the factor processes are first marginalized out and the factor loadings are estimated by the maximum marginal likelihood

estimator. Various studies considered the space-varying factor loadings through certain basis functions, such as local bisquare functions (Cressie and Johannesson, 2008; Ma and Kang, 2017), wavelets (Shi and Cressie, 2007), and orthonormalized cubic B-splines (Chu et al., 2014). It is interesting to compare the performance of these approaches. Furthermore, in estimating the factor loadings, we only use the observations on  $\mathbf{s}^{\mathcal{D}}$ . It may be more satisfying to develop a method to use all data, including  $\mathbf{y}(\mathbf{s}^*)$ , to estimate the factor loadings.

## Acknowledgements

The research of Mengyang Gu was part of his PhD thesis at Duke University. The authors thank the editor, the associate editor and two referees for their comments that substantially improved the article. The authors sincerely thank Barbara Engelhardt for providing the methylation level data and discussion.

## Appendix: Proofs for Section 2

*Proof of Lemma 1.* Because  $\mathbf{A} = \mathbf{U}\mathbf{D}/\sqrt{n}$ ,  $\mathbf{A}(\mathbf{A}^T\mathbf{A})^{-1}\mathbf{A}^T = \mathbf{I}_K$ . The likelihood is

$$\begin{aligned} p(\mathbf{Y}_v(\mathbf{s}^{\mathcal{D}})|\mathbf{v}_v(\mathbf{s}^{\mathcal{D}}), \sigma_0^2) &= (2\pi\sigma_0^2)^{-nK/2} \exp\left(-\frac{(\mathbf{Y}_v(\mathbf{s}^{\mathcal{D}}) - \mathbf{A}_v\mathbf{v}_v(\mathbf{s}^{\mathcal{D}}))^T (\mathbf{Y}_v(\mathbf{s}^{\mathcal{D}}) - \mathbf{A}_v\mathbf{v}_v(\mathbf{s}^{\mathcal{D}}))}{2\sigma_0^2}\right) \\ &= (2\pi\sigma_0^2)^{-nK/2} \exp\left(-\frac{(\hat{\mathbf{v}}_v(\mathbf{s}^{\mathcal{D}}) - \mathbf{v}_v(\mathbf{s}^{\mathcal{D}}))^T \mathbf{A}_v^T \mathbf{A}_v (\hat{\mathbf{v}}_v(\mathbf{s}^{\mathcal{D}}) - \mathbf{v}_v(\mathbf{s}^{\mathcal{D}}))}{2\sigma_0^2}\right), \end{aligned}$$

where  $\hat{\mathbf{v}}_v(\mathbf{s}^{\mathcal{D}}) = (\mathbf{A}_v^T \mathbf{A}_v)^{-1} \mathbf{A}_v^T \mathbf{Y}_v(\mathbf{s}^{\mathcal{D}})$ .  $\mathbf{A}_v^T \mathbf{A}_v$  is a diagonal matrix because

$$\mathbf{A}_v^T \mathbf{A}_v = \begin{pmatrix} (\mathbf{I}_n \otimes \mathbf{a}_1)^T (\mathbf{I}_n \otimes \mathbf{a}_1) & (\mathbf{I}_n \otimes \mathbf{a}_1)^T (\mathbf{I}_n \otimes \mathbf{a}_2) & \dots & (\mathbf{I}_n \otimes \mathbf{a}_1)^T (\mathbf{I}_n \otimes \mathbf{a}_K) \\ (\mathbf{I}_n \otimes \mathbf{a}_2)^T (\mathbf{I}_n \otimes \mathbf{a}_1) & (\mathbf{I}_n \otimes \mathbf{a}_2)^T (\mathbf{I}_n \otimes \mathbf{a}_2) & \dots & (\mathbf{I}_n \otimes \mathbf{a}_2)^T (\mathbf{I}_n \otimes \mathbf{a}_K) \\ \dots & \dots & \dots & \dots \\ (\mathbf{I}_n \otimes \mathbf{a}_K)^T (\mathbf{I}_n \otimes \mathbf{a}_1) & (\mathbf{I}_n \otimes \mathbf{a}_K)^T (\mathbf{I}_n \otimes \mathbf{a}_2) & \dots & (\mathbf{I}_n \otimes \mathbf{a}_K)^T (\mathbf{I}_n \otimes \mathbf{a}_K) \end{pmatrix},$$

with  $(\mathbf{I}_n \otimes \mathbf{a}_i)^T (\mathbf{I}_n \otimes \mathbf{a}_i) = (\mathbf{I}_n^T \otimes \mathbf{a}_i^T) (\mathbf{I}_n \otimes \mathbf{a}_i) = (\mathbf{I}_n^T \mathbf{I}_n) \otimes (\mathbf{a}_i^T \mathbf{a}_i)$  and  $(\mathbf{I}_n \otimes \mathbf{a}_i)^T (\mathbf{I}_n \otimes \mathbf{a}_j) = (\mathbf{I}_n^T \mathbf{I}_n) \otimes (\mathbf{a}_i^T \mathbf{a}_j) = \mathbf{O}$ , where  $\mathbf{O}$  is a matrix with each element being 0. Marginalizing out  $\mathbf{v}_v(\mathbf{s}^{\mathcal{D}})$ , one has

$$\begin{aligned} & p(\mathbf{Y}_v(\mathbf{s}^{\mathcal{D}}) | \sigma_0^2, \boldsymbol{\tau}_{1:K}^2, \boldsymbol{\gamma}_{1:K}, \boldsymbol{\eta}_{1:K}) \\ &= \int p(\mathbf{Y}_v(\mathbf{s}^{\mathcal{D}}) | \hat{\mathbf{v}}_v(\mathbf{s}^{\mathcal{D}}), \sigma_0^2) p(\hat{\mathbf{v}}_v(\mathbf{s}^{\mathcal{D}}) | \boldsymbol{\tau}_{1:K}^2, \boldsymbol{\gamma}_{1:K}, \boldsymbol{\eta}_{1:K}) d\hat{\mathbf{v}}_v(\mathbf{s}^{\mathcal{D}}) \\ &= |\mathbf{A}_v^T \mathbf{A}_v|^{-1/2} (2\pi)^{-nK/2} |\boldsymbol{\Sigma}_v + \sigma_0^2 (\mathbf{A}_v^T \mathbf{A}_v)^{-1}|^{-1/2} \exp\left(-\frac{1}{2} \hat{\mathbf{v}}_v(\mathbf{s}^{\mathcal{D}})^T (\boldsymbol{\Sigma}_v + \sigma_0^2 (\mathbf{A}_v^T \mathbf{A}_v)^{-1})^{-1} \hat{\mathbf{v}}_v(\mathbf{s}^{\mathcal{D}})\right) \\ &= |\mathbf{A}_v^T \mathbf{A}_v|^{-1/2} \times \\ & \quad \prod_{i=1}^K \left\{ (2\pi)^{-n/2} |\sigma_i^2 \tilde{\mathbf{R}}_i + \sigma_0^2 (\mathbf{a}_i^T \mathbf{a}_i)^{-1} \mathbf{I}_n|^{-1/2} \exp\left(-\frac{1}{2} \hat{\mathbf{v}}_i(\mathbf{s}^{\mathcal{D}})^T (\sigma_i^2 \tilde{\mathbf{R}}_i + \sigma_0^2 (\mathbf{a}_i^T \mathbf{a}_i)^{-1} \mathbf{I}_n)^{-1} \hat{\mathbf{v}}_i(\mathbf{s}^{\mathcal{D}})\right) \right\}. \end{aligned}$$

The last row follows from the fact that  $\hat{\mathbf{v}}_i(\mathbf{s}^{\mathcal{D}})^T$  is the  $l^{\text{th}}$  row of the matrix  $\hat{\mathbf{v}}(\mathbf{s}^{\mathcal{D}})$ .  $\square$

*Proof of Lemma 2.* Denote  $\mathbf{Y}(\mathbf{s}^{\mathcal{D}}; s_j^*) := [\mathbf{Y}(\mathbf{s}^{\mathcal{D}}); Y(s_j^*)]$  and  $\mathbf{v}(\mathbf{s}^{\mathcal{D}}; s_j^*) := [\mathbf{v}(\mathbf{s}^{\mathcal{D}}); v(s_j^*)]$ . Both are  $k \times (n+1)$  matrices.

Vectorizing the output  $\mathbf{Y}_v(\mathbf{s}^{\mathcal{D}}, s_j^*) := \text{vec}(\mathbf{Y}(\mathbf{s}^{\mathcal{D}}, s_j^*))$ , a  $K \times (n+1)$  vector, and  $\mathbf{v}_v(\mathbf{s}^{\mathcal{D}}) := \text{vec}(\mathbf{v}(\mathbf{s}^{\mathcal{D}})^T)$ , we can write model (1) as,

$$\mathbf{Y}_v(\mathbf{s}^{\mathcal{D}}, s_j^*) = \mathbf{A}_v \mathbf{v}_v(\mathbf{s}^{\mathcal{D}}, s_j^*) + \boldsymbol{\epsilon},$$

where  $\boldsymbol{\epsilon} \sim \text{MN}(\mathbf{0}, \sigma_0^2 \mathbf{I}_{(n+1)K})$ . Similar to the proof of Lemma 1, one has

$$p(\mathbf{Y}_v(\mathbf{s}^{\mathcal{D}}, s_j^*) \mid \boldsymbol{\sigma}_0^2, \boldsymbol{\tau}_{1:K}^2, \boldsymbol{\gamma}_{1:K}, \boldsymbol{\eta}_{1:K}) = |\mathbf{A}_v^T \mathbf{A}_v|^{-1/2} \prod_{i=1}^K p_{MN}(\hat{\mathbf{v}}_i(\mathbf{s}^{\mathcal{D}}, s_j^*); \mathbf{0}, \sigma_i^2 \boldsymbol{\Lambda}_i + \sigma_0^2 (\mathbf{a}_i^T \mathbf{a}_i)^{-1} \mathbf{I}_{n+1}),$$

where  $\hat{\mathbf{v}}_i(\mathbf{s}^{\mathcal{D}}, s_j^*)$  is the transpose of the  $l^{\text{th}}$  row of the  $\hat{\mathbf{v}}(\mathbf{s}^{\mathcal{D}}, s_j^*) := (\mathbf{A}^T \mathbf{A})^{-1} \mathbf{A}^T \mathbf{Y}(\mathbf{s}^{\mathcal{D}}, s_j^*)$  and

$$\boldsymbol{\Lambda}_i = \begin{pmatrix} \tilde{\mathbf{R}}_i & \mathbf{r}_i(s_j^*) \\ \mathbf{r}_i^T(s_j^*) & \tilde{c}_i(s_j^*, s_j^*) \end{pmatrix}. \text{ One has}$$

$$(\hat{v}_i(s_j^*) \mid \hat{\mathbf{v}}_i(\mathbf{s}^{\mathcal{D}}), \boldsymbol{\sigma}_0^2, \tau_i^2, \gamma_i, \eta_i) \sim \text{N}(\hat{v}_i^*(s_j^*), \sigma_i^2 \tilde{c}^*(s_j^*) + \sigma_0^2 (\mathbf{a}_i^T \mathbf{a}_i)^{-1}), \quad (22)$$

with  $\hat{v}_i^*(s_j^*) = \mathbf{r}_i^T(s_j^*) (\tilde{\mathbf{R}}_i + \frac{\sigma_0^2 (\mathbf{a}_i^T \mathbf{a}_i)^{-1}}{\tau_i^2} \mathbf{I}_n)^{-1} \hat{\mathbf{v}}_i(\mathbf{s}^{\mathcal{D}})$  and  $\tilde{c}_i^*(s_j^*) = \tilde{c}_i(s_j^*, s_j^*) - \mathbf{r}_i^T(s_j^*) (\tilde{\mathbf{R}}_i + \frac{\sigma_0^2 (\mathbf{a}_i^T \mathbf{a}_i)^{-1}}{\tau_i^2} \mathbf{I}_n)^{-1} \mathbf{r}_i(s_j^*)$ .

Note  $\mathbf{A}(\mathbf{A}^T \mathbf{A})^{-1} \mathbf{A}^T = \mathbf{I}_K$ . One has  $\mathbf{Y}(s_j^*) = \mathbf{A} \hat{\mathbf{v}}(s_j^*)$  and  $\mathbf{Y}(s^{\mathcal{D}}) = \mathbf{A} \hat{\mathbf{v}}(s^{\mathcal{D}})$ . Applying the properties of multivariate normal distribution to (22) leads to the results.

□

## References

- Banerjee, S., Gelfand, A. E., Finley, A. O., and Sang, H. (2008). Gaussian predictive process models for large spatial data sets. *Journal of the Royal Statistical Society: Series B (Statistical Methodology)*, 70(4):825–848.
- Bayarri, M. J., Berger, J. O., Calder, E. S., Dalbey, K., Lunagomez, S., Patra, A. K., Pitman, E. B., Spillerh, E. T., and Wolperti, R. L. (2009). Using statistical and computer models to quantify volcanic hazards. *Technometrics*, 51:402–413.
- Breiman, L. (2001). Random forests. *Machine learning*, 45(1):5–32.
- Chang, W., Haran, M., Olson, R., Keller, K., et al. (2014). Fast dimension-reduced climate

- model calibration and the effect of data aggregation. *The Annals of Applied Statistics*, 8(2):649–673.
- Chu, T., Wang, H., and Zhu, J. (2014). On semiparametric inference of geostatistical models via local karhunen–loève expansion. *Journal of the Royal Statistical Society: Series B (Statistical Methodology)*, 76(4):817–832.
- Conti, S. and O’Hagan, A. (2010). Bayesian emulation of complex multi-output and dynamic computer models. *Journal of statistical planning and inference*, 140(3):640–651.
- Cressie, N. and Johannesson, G. (2008). Fixed rank kriging for very large spatial data sets. *Journal of the Royal Statistical Society: Series B (Statistical Methodology)*, 70(1):209–226.
- Das, P. M. and Singal, R. (2004). DNA methylation and cancer. *Journal of clinical oncology*, 22(22):4632–4642.
- Eidsvik, J., Shaby, B. A., Reich, B. J., Wheeler, M., and Niemi, J. (2013). Estimation and prediction in spatial models with block composite likelihoods. *Journal of Computational and Graphical Statistics*, (just-accepted).
- Gelfand, A. E., Diggle, P., Guttorp, P., and Fuentes, M. (2010). *Handbook of spatial statistics*. CRC Press.
- Gelfand, A. E., Schmidt, A. M., Banerjee, S., and Sirmans, C. (2004). Nonstationary multivariate process modeling through spatially varying coregionalization. *Test*, 13(2):263–312.
- Goulard, M. and Voltz, M. (1992). Linear coregionalization model: tools for estimation and choice of cross-variogram matrix. *Mathematical Geology*, 24(3):269–286.
- Gu, M. (2019a). *FastGaSP: Fast and Exact Computation of Gaussian Stochastic Process*. R package version 0.5.1.

- Gu, M. (2019b). Jointly robust prior for Gaussian stochastic process in emulation, calibration and variable selection. *Bayesian Analysis*, 14(3):857–885.
- Gu, M. and Berger, J. O. (2016). Parallel partial Gaussian process emulation for computer models with massive output. *Annals of Applied Statistics*, 10(3):1317–1347.
- Gu, M. and Shen, W. (2018). Generalized probabilistic principal component analysis of correlated data. *arXiv preprint arXiv:1808.10868*.
- Gu, M., Wang, X., and Berger, J. O. (2018). Robust Gaussian stochastic process emulation. *Annals of Statistics*, 46(6A):3038–3066.
- Hartikainen, J. and Sarkka, S. (2010). Kalman filtering and smoothing solutions to temporal Gaussian process regression models. In *Machine Learning for Signal Processing (MLSP), 2010 IEEE International Workshop on*, pages 379–384. IEEE.
- Higdon, D., Gattiker, J., Williams, B., and Rightley, M. (2008). Computer model calibration using high-dimensional output. *Journal of the American Statistical Association*, 103(482):570–583.
- Kaufman, C. G., Schervish, M. J., and Nychka, D. W. (2008). Covariance tapering for likelihood-based estimation in large spatial data sets. *Journal of the American Statistical Association*, 103(484):1545–1555.
- Liaw, A. and Wiener, M. (2002). Classification and regression by randomforest. *R News*, 2(3):18–22.
- Lindgren, F., Rue, H., and Lindström, J. (2011). An explicit link between gaussian fields and gaussian markov random fields: the stochastic partial differential equation approach. *Journal of the Royal Statistical Society: Series B (Statistical Methodology)*, 73(4):423–498.

- Ma, P. and Kang, E. L. (2017). Fused Gaussian process for very large spatial data. *arXiv preprint arXiv:1702.08797*.
- Petris, G., Petrone, S., and Campagnoli, P. (2009). *Dynamic linear models*. Springer.
- R Core Team (2019). *R: A Language and Environment for Statistical Computing*. R Foundation for Statistical Computing, Vienna, Austria.
- Sacks, J., Welch, W. J., Mitchell, T. J., and Wynn, H. P. (1989). Design and analysis of computer experiments. *Statistical science*, 4(4):409–423.
- Scarano, M. I., Strazzullo, M., Matarazzo, M. R., and D’Esposito, M. (2005). DNA methylation 40 years later: Its role in human health and disease. *Journal of cellular physiology*, 204(1):21–35.
- Shi, T. and Cressie, N. (2007). Global statistical analysis of misr aerosol data: a massive data product from nasa’s terra satellite. *Environmetrics: The official journal of the International Environmetrics Society*, 18(7):665–680.
- West, M. and Harrison, P. J. (1997). *Bayesian Forecasting & Dynamic Models*. Springer Verlag, 2nd edition.
- Whittle, P. (1954). On stationary processes in the plane. *Biometrika*, pages 434–449.
- Whittle, P. (1963). Stochastic process in several dimensions. *Bulletin of the International Statistical Institute*, 40(2):974–994.
- Wickham, H. (2007). Reshaping data with the reshape package. *Journal of Statistical Software*, 21(12):1–20.
- Wickham, H. (2016). *ggplot2: Elegant Graphics for Data Analysis*. Springer-Verlag New York.



Zhang, W., Spector, T. D., Deloukas, P., Bell, J. T., and Engelhardt, B. E. (2015). Predicting genome-wide DNA methylation using methylation marks, genomic position, and dna regulatory elements. *Genome biology*, 16(14):1–20.

Ziller, M. J., Gu, H., Müller, F., Donaghey, J., Tsai, L. T.-Y., Kohlbacher, O., De Jager, P. L., Rosen, E. D., Bennett, D. A., Bernstein, B. E., et al. (2013). Charting a dynamic DNA methylation landscape of the human genome. *Nature*, 500(7463):477–481.

# Supplementary materials

All the formulas in this supplementary materials are cross-referenced in the main body of the article.

## S1 Closed form quantities of the continuous state space model

We give the quantities of continuous state space model representation in (11) in the main body of the article.

For  $1 \leq i \leq K$ , the SDE is

$$\frac{d\boldsymbol{\theta}_i(s)}{ds} = \mathbf{J}_i \boldsymbol{\theta}_i(s) + \mathbf{L}z(s),$$

where

$$\mathbf{J}_i = \begin{pmatrix} 0 & 1 & 0 \\ 0 & 0 & 1 \\ -\lambda_i^3 & -\lambda_i^2 & -3\lambda_i \end{pmatrix},$$

and  $\mathbf{L} = (0, 0, 1)^T$ .

Denote  $d_j = |s_{j+1} - s_j|$  for  $j = 1, \dots, N - 1$ . We have the following expressions for the solution of the SDE in (11) in the main body of the article,

$$\mathbf{G}_i(s_j) = e^{\mathbf{J}_i d_j} = \frac{e^{-\lambda_i d_j}}{2} \begin{pmatrix} \lambda_i^2 d_j^2 + 2\lambda_i + 2 & 2(\lambda_i d_j^2 + d_j) & d_j^2 \\ -\lambda_i^3 d_j^2 & -2(\lambda_i^2 d_j^2 - \lambda_i d_j - 1) & 2d_j - \lambda_i d_j^2 \\ \lambda_i^4 d_j^2 - 2\lambda_i^3 d_j & 2(\lambda_i^3 d_j^2 - 3\lambda_i^2 d_j) & \lambda_i^2 d_j^2 - 4\lambda_i d_j + 2 \end{pmatrix}$$

$$\mathbf{W}_i(s_j) = \frac{4\sigma_i^2\lambda_i^5}{3} \begin{pmatrix} W_{1,i}(s_j) & W_{2,i}(s_j) & W_{3,i}(s_j) \\ W_{4,i}(s_j) & W_{5,i}(s_j) & W_{6,i}(s_j) \\ W_{7,i}(s_j) & W_{8,i}(s_j) & W_{9,i}(s_j) \end{pmatrix},$$

with

$$\begin{aligned} W_{1,i}(s_j) &= \frac{e^{-2\lambda_i d_j} (3 + 6\lambda_i d_j + 6\lambda_i^2 d_j^2 + 4\lambda_i^3 d_j^3 + 2\lambda_i^4 d_j^4) - 3}{-4\lambda_i^5}, \\ W_{2,i}(s_j) &= W_{4,i}(s_j) = \frac{e^{-2\lambda_i d_j} d_j^4}{2}, \\ W_{3,i}(s_j) &= W_{7,i}(s_j) = \frac{e^{-2\lambda_i d_j} (1 + 2\lambda_i d_j + 2\lambda_i^2 d_j^2 + 4\lambda_i^3 d_j^3 - 2\lambda_i^4 d_j^4) - 1}{4\lambda_i^3}, \\ W_{5,i}(s_j) &= \frac{e^{-2\lambda_i d_j} (1 + 2\lambda_i d_j + 2\lambda_i^2 d_j^2 - 4\lambda_i^3 d_j^3 + 2\lambda_i^4 d_j^4) - 1}{-4\lambda_i^3}, \\ W_{6,i}(s_j) &= W_{8,i}(s_j) = \frac{e^{-2\lambda_i d_j} d_j^2 (4 - 4\lambda_i d_j + \lambda_i^2 d_j^2)}{2}, \\ W_{9,i}(s_j) &= \frac{e^{-2\lambda_i d_j} (-3 + 10\lambda_i^2 d_j^2 - 22\lambda_i^2 d_j^2 + 12\lambda_i^2 d_j^2 - 2\lambda_i^4 d_j^4) + 3}{4\lambda_i}, \end{aligned}$$

and

$$\mathbf{W}_i(s_0) = \begin{pmatrix} \sigma_i^2 & 0 & -\sigma_i^2\lambda_i^2/3 \\ 0 & \sigma_i^2\lambda_i^2/3 & 0 \\ -\sigma_i^2\lambda_i^2/3 & 0 & \sigma_i^2\lambda_i^4 \end{pmatrix},$$

for  $j = 1, \dots, N$  and  $i = 1, \dots, K$ .

For  $i = 1, \dots, K$ , the joint distribution of  $\boldsymbol{\theta}_i(s_{0:N})$  is given below

$$\begin{pmatrix} \boldsymbol{\theta}_i(s_0) \\ \boldsymbol{\theta}_i(s_1) \\ \boldsymbol{\theta}_i(s_2) \\ \dots \\ \boldsymbol{\theta}_i(s_N) \end{pmatrix} \sim \text{MN}(\mathbf{0}_N, \boldsymbol{\Lambda}^{-1}),$$

where

$$\mathbf{\Lambda} = \begin{pmatrix} \mathbf{W}_i^{-1}(s_0) + \mathbf{G}_i^T(s_1)\mathbf{W}_i^{-1}(s_1)\mathbf{G}_i(s_1) & -\mathbf{G}_i^T(s_1)\mathbf{W}_i^{-1}(s_1) & & & \\ -\mathbf{W}_i^{-1}(s_1)\mathbf{G}_i(s_1) & \mathbf{W}_i^{-1}(s_1) + \mathbf{G}_i^T(s_1)\mathbf{W}_i^{-1}(s_2)\mathbf{G}_i(s_1) & & & \\ & -\mathbf{W}_i^{-1}(s_2)\mathbf{G}_i(s_2) & \dots & & \\ & \dots & \dots & \dots & -\mathbf{G}_i^T(s_N)\mathbf{W}_i^{-1}(s_N) \\ & \dots & & & \mathbf{W}_i^{-1}(s_N) \\ & & & -\mathbf{W}_i^{-1}(s_N)\mathbf{G}_i(s_N) & \end{pmatrix}$$

## S2 Combing feature data into the nonseparable model

To impute the methylation levels, some site-specific features such as genomic position, DNA sequence properties, cis-regulatory element, can be used as covariates in a regression model. Incorporating regressors/covariates is less studied in the nonseparable GaSP model. In this section, we discuss a way to jointly model the site-specific features and output.

Let  $\mathbf{X}(s)_{[q \times 1]}$  be features at site  $s$  (including the intercept). Consider an extended model

$$\mathbf{Y}^e(s) = \mathbf{A}^e \tilde{\mathbf{v}}(s) + \boldsymbol{\epsilon}_0, \quad (\text{S1})$$

for every  $s \in \mathcal{S}$ , where  $\mathbf{Y}^e(s) = (\mathbf{X}^T(s); \mathbf{Y}^T(s))^T$ , the weight  $\tilde{\mathbf{v}}(\cdot)$  is defined the same as in (2) in the main body of the article, and  $\boldsymbol{\epsilon}_0 \sim \text{MN}(0, \sigma_0^2 \mathbf{I}_{K+q})$ . Let  $\mathbf{X}(\mathbf{s}^{\mathcal{S}})_{[q \times n]}$  be the features at sites  $\mathbf{s}^{\mathcal{S}}$  and  $\mathbf{Y}^e(\mathbf{s}^{\mathcal{S}}) = (\mathbf{X}^T(\mathbf{s}^{\mathcal{S}}); \mathbf{Y}^T(\mathbf{s}^{\mathcal{S}}))^T$ . The extended basis matrix  $\mathbf{A}^e = \mathbf{U}^e \mathbf{D}^e / \sqrt{n}$ , where  $\mathbf{U}^e$  and  $\mathbf{D}^e$  are still defined through the SVD decomposition  $\mathbf{Y}^e(\mathbf{s}^{\mathcal{S}}) = \mathbf{U}^e \mathbf{D}^e \mathbf{V}^e$ . The predictive distribution of the model (S1) can be obtained similarly to Lemma 2.

The connection among regression model, the separable GaSP model, and the nonseparable GaSP model shown in the previous section still holds. Let  $\mathbf{Z}^e$  follow a matrix normal distribution with mean zero and covariance  $\boldsymbol{\Sigma}^e \otimes \mathbf{\Lambda}$ , where  $\boldsymbol{\Sigma}^e = \begin{pmatrix} \boldsymbol{\Sigma}_{00}^e & \boldsymbol{\Sigma}_{0*}^e \\ \boldsymbol{\Sigma}_{*0}^e & \boldsymbol{\Sigma}_{**}^e \end{pmatrix}$  is a  $(q+K) \times (q+K)$  covariance matrix. The separable model is a special case of the nonseparable GaSP model (S1) specified in Remark 2. The prediction by the regression model (19) with covariates  $\mathbf{H}_i(s_j) = (\mathbf{X}^T(s_j); \mathbf{y}^T(s_j))^T$  is also a special case of the extended nonseparable

25% held-out CpG sites	RMSE	$P_{CI}(95\%)$	$L_{CI}(95\%)$	Accuracy
Nonseparable GaSP full model	0.083	0.956	0.278	0.969
Nonseparable GaSP by batch	0.091	0.923	0.258	0.966
75% held-out CpG sites	RMSE	$P_{CI}(95\%)$	$L_{CI}(95\%)$	Accuracy
Nonseparable GaSP full model	0.087	0.963	0.305	0.968
Nonseparable GaSP by batch	0.096	0.934	0.283	0.966

Table S1: Comparison of different methods in terms of out of sample prediction for WGBS data with 25% and 75% CpG sites are held out for testing.

GaSP model specified in Remark 1.

### S3 Comparison to approximation method by blocks

In this subsection, we compare our exact and fast computation of the nonseparable GaSP model with a straightforward approximation, in which the long sequence is divided into small blocks and GaSP models are built independently in each block. Assume the data are divided into  $M$  blocks, each with  $n_0$  inputs (where  $n = Mn_0$ ), the computational operations of which are then  $O(Mn_0^3)$  instead of  $O(n^3)$  for the inversion of the covariance matrix.

For illustration purposes, the data are divided into 100 batches and 200 CpG sites are used as the training data in each batch. We consider two scenarios, with 600 CpG sites and 66 CpG sites between these 200 CpG sites being selected as the test CpG sites in each batch, respectively. That means that roughly 75% and 25% of the data are held out. We still assume the methylation levels for the first 20 samples are available at all CpG sites and 4 randomly selected samples are only partially observed. The total number of the test CpG sites is 240,000 and 26,400, respectively.

As shown in Table S1, the prediction by the nonseparable GaSP with the full model is about 10% better in terms of RMSE in both scenarios. This is further justified by Figure S1. One possible reason is that the boundary effect is large in the approximation method when we divide the data into batches. All these results suggest that simply approximating the

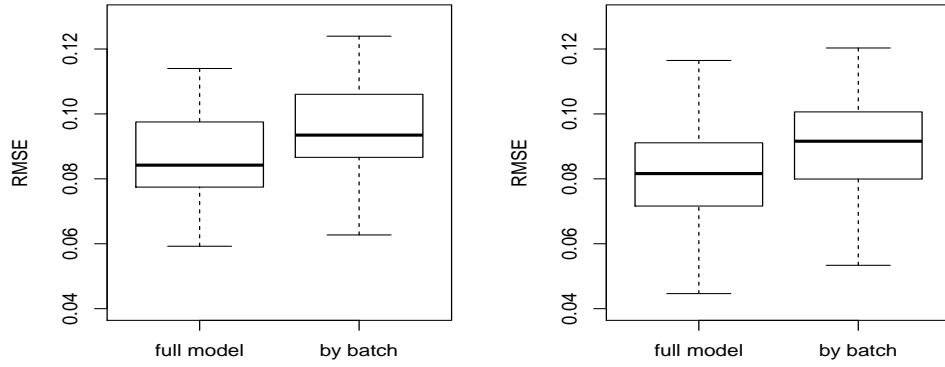


Figure S1: Boxplots of  $RMSE_j$  for the test samples in batch  $j$  with 75% of CpG sites (left panel) and 25% of CpG sites (right panel) being held-out, respectively,  $j = 1, \dots, 100$ .

likelihood by batch yields inferior predictive results than the nonseparable GaSP model with the full likelihood. Again, the implementation of the full model relies on the FFBS algorithm discussed in Section 3 in the main body of the article.